

**FEMTOSECOND OPTICAL PARAMETRIC  
AMPLIFIERS BASED ON BETA-BARIUM BORATE  
CRYSTALS**

A THESIS

SUBMITTED TO THE DEPARTMENT OF ELECTRICAL AND  
ELECTRONICS ENGINEERING  
AND THE INSTITUTE OF ENGINEERING AND SCIENCES  
OF BILKENT UNIVERSITY  
IN PARTIAL FULFILLMENT OF THE REQUIREMENTS  
FOR THE DEGREE OF  
MASTER OF SCIENCE

By

**Kahraman Güçlü Köprülü**

**September 1996**

THESIS  
TK  
7871.2  
.K67  
1996

FEMTOSECOND OPTICAL PARAMETRIC  
AMPLIFIERS BASED ON BETA-BARIUM BORATE  
CRYSTALS

A THESIS

SUBMITTED TO THE DEPARTMENT OF ELECTRICAL AND  
ELECTRONICS ENGINEERING

AND THE INSTITUTE OF ENGINEERING AND SCIENCES  
OF BILKENT UNIVERSITY

IN PARTIAL FULFILLMENT OF THE REQUIREMENTS  
FOR THE DEGREE OF  
MASTER OF SCIENCE

By

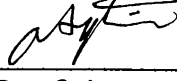
Kahraman Güçlü Köprülü

September 1996

TK  
7871.2  
·K67  
1996

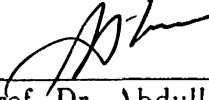
B.03.233

I certify that I have read this thesis and that in my opinion it is fully adequate,  
in scope and in quality, as a thesis for the degree of Master of Science.



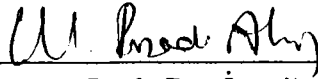
Assist. Prof. Dr. Orhan Aytür (Supervisor)

I certify that I have read this thesis and that in my opinion it is fully adequate,  
in scope and in quality, as a thesis for the degree of Master of Science.



Prof. Dr. Abdullah Atalar

I certify that I have read this thesis and that in my opinion it is fully adequate,  
in scope and in quality, as a thesis for the degree of Master of Science.



Assoc. Prof. Dr. İrşadi Aksun

Approved for the Institute of Engineering and Sciences:



Prof. Dr. Mehmet Baray  
Director of Institute of Engineering and Sciences

## ABSTRACT

# FEMTOSECOND OPTICAL PARAMETRIC AMPLIFIERS BASED ON BETA-BARIUM BORATE CRYSTALS

Kahraman Güçlü Köprülü  
M.S. in Electrical and Electronics Engineering  
Supervisor: Assist. Prof. Dr. Orhan Aytür  
September 1996

In this thesis we describe our experiments to construct and evaluate non-degenerate and degenerate optical parametric amplifiers (OPA) based on beta-barium borate (BBO) crystals. We used a mode-locked Titanium:Sapphire laser at a wavelength of 830 nm and a pulse duration of 140 fs. The Ti:Sapphire laser was frequency doubled with a type-I BBO crystal. The frequency doubled output of the laser was used to pump our OPAs. For 800 mW of laser output, 300 mW of maximum output power at the second harmonic was obtained, corresponding to a 38% conversion efficiency. Both type-I and type-II BBO crystals were used for parametric amplification. The type-II crystal resulted in a nondegenerate OPA due to the orthogonal polarizations of the signal and the idler beams. A degenerate OPA was achieved with the type-I crystal. Phase sensitive nature of the degenerate OPA, and phase insensitive nature of the nondegenerate OPA were observed. The maximum gain of the degenerate OPA was measured to be 1.45, whereas the maximum gain of the nondegenerate OPA was measured to be 1.02.

*Keywords:* optical parametric amplification, parametric gain, nonlinear crystals, BBO, second harmonic generation, ultrafast lasers, Ti:Sapphire.

## ÖZET

### BETA-BARYUM BORAT KRİSTALİ TEMELLİ FEMTOSANİYE OPTİK PARAMETİK YÜKSELTİCİLER

Kahraman Güçlü Köprülü  
Elektrik ve Elektronik Mühendisliği Bölümü Yüksek Lisans  
Tez Yöneticisi: Yar. Doç. Dr. Orhan Aytür  
Eylül 1996

Bu tezde, dejenere ve dejenere-olmayan beta-baryum borat (BBO) kristali bazlı optik parametrik yükselticiler (OPA) oluşturmak ve değerlendirmek için yaptığımız deneysel çalışmalar anlatılmaktadır. Dalga boyu 830 nm ve darbe uzunluğu 140 fs olan bir Titanyum:Safir lazeri kullandık. Tip-I BBO kristali kullanarak Ti:Safir lazerinin frekansı ikiye katlanmıştır. Frekansı katlanmış lazer ışını OPA'ları pompalamak için kullanılmıştır. 800 mW lazer çıkışı için %38 dönüşüm verimine karşılık gelen en yüksek 300 mW ikinci harmonik elde edilmiştir. Parametrik yükseltme için hem tip-I hem de tip-II BBO kristali kullanılmıştır. Tip-II BBO kristali sinyal ve fazlalık ışınlarının birbirlerine dik polarizasyonları yüzünden dejenere-olmayan parametrik yükseltme sağlamıştır. Tip-I kristal ile dejenere bir OPA başarılmıştır. Dejenere OPA'nın faza bağımlılığı ve dejenere-olmayan OPA'nın fazdan bağımsızlığı gözlenmiştir. Dejenere OPA'nın en yüksek kazancı 1.45, dejenere-olmayan OPA'nınki ise 1.02 olarak ölçülmüştür.

*Anahtar kelimeler:* optik parametrik yükseltme, parametrik kazanç, doğrusal olmayan kristaller, BBO, ikinci harmonik üretimi, ultra hızlı lazerler, Titanyum:Safir.

## ACKNOWLEDGMENTS

I would like to express my sincere gratitude to Dr. Orhan Aytür for his supervision, guidance, suggestion, and especially encouragement through the development of this thesis.

I would like to thank Dr. Abdullah Atalar and Dr. İrşadi Aksun for reading the manuscript and commenting on the thesis.

I am indebted to Tolga Kartalođlu for his help during the development of the thesis and experimental work.

I would like to thank İlhan Altuđ and Serdal Elver of Bilkent University's Purchasing Department, and Mürüvet Parlakay for all their help.

I would also like to express my thanks to the Turkish Scientific and Technical Research Council and NATO for their partial support of this work under Grant No. EEEAG-118 and Grant No. TU-MIMIC, respectively.

# TABLE OF CONTENTS

|          |   |           |
|----------|---|-----------|
| <b>1</b> | <b>INTRODUCTION</b>   | <b>1</b>  |
| <b>2</b> | <b>THEORY OF OPTICAL PARAMETRIC AMPLIFICATION</b>               | <b>4</b>  |
| 2.1      | Nonlinear Materials . . . . .                                   | 4         |
| 2.2      | Three Wave Mixing in Second-Order Nonlinear Materials . . . . . | 6         |
| 2.3      | Nondegenerate Optical Parametric Amplification                  | 9         |
| 2.4      | Degenerate Optical Parametric Amplification . . . . .           | 14        |
| 2.5      | Second Harmonic Generation                                      | 16        |
| 2.6      | Phase Matching . . . . .  | 18        |
| <b>3</b> | <b>EXPERIMENTAL WORK</b>  | <b>22</b> |
| 3.1      | The Laser . . . . .   | 23        |
| 3.2      | Beta-Barium Borate Crystal . . . . .                            | 24        |
| 3.3      | Second Harmonic Generation                                      | 27        |
| 3.4      | Optical Parametric Amplification . . . . .                      | 30        |
| 3.4.1    | The Pump Beam . . . . .   | 30        |
| 3.4.2    | Parametric Amplification Using Focused Gaussian Beams           | 31        |
| 3.4.3    | Effect of Group Velocity Mismatch . . . . .                     | 33        |
| 3.4.4    | Detection of Ultrashort Pulses . . . . .                        | 33        |



|          |  |           |
|----------|--|-----------|
| 3.4.5    | Degenerate Optical Parametric Amplification    | 34        |
| 3.4.6    | Nondegenerate Optical Parametric Amplification | 38        |
| <b>4</b> | <b>CONCLUSIONS</b>                             | <b>42</b> |

## LIST OF FIGURES

|     |  |    |
|-----|--|----|
| 2.1 | Schematic and energy diagram for optical parametric amplification. . . . .   | 10 |
| 2.2 | Spatial evolution of signal and idler field intensities for a nondegenerate optical parametric amplifier for the case of no phase mismatch in the constant pump approximation. . . . .                                 | 11 |
| 2.3 | Dependence of parametric gain on the pump field intensity for constant length of interaction. . . . .  | 12 |
| 2.4 | The signal gain of a nondegenerate optical parametric amplifier as a function of $\Delta k$ . . . . .  | 13 |
| 2.5 | Spatial evolution of signal and idler and pump photon fluxes for nondegenerate optical parametric amplifier for the case of no phase mismatch. . . . .   | 14 |
| 2.6 | Parametric gain of nondegenerate optical parametric amplifier (NOPA) and degenerate optical parametric amplifier (DOPA) when $\kappa L = 1$ as a function of phase difference between the pump and the signal. . . . . | 16 |
| 2.7 | Schematic and energy diagram for second harmonic generation. . . . .   | 17 |
| 2.8 | Spatial evolution of the fundamental and second harmonic field intensities for the case of perfect phase matching and the boundary condition of no second harmonic field at the input. . . . .                         | 18 |
| 2.9 | Directions of polarizations for $\omega_1$ , $\omega_2$ , and $\omega_3$ for type-I and type-II phase matching in three wave mixing ( $\omega_1 + \omega_2 = \omega_3$ ). . . . .                                      | 19 |

|      |   |    |
|------|---|----|
| 2.10 | $\theta$ and $\phi$ angles defined due to spherical coordinates. . . . .  | 20 |
| 3.1  | Schematic of the optical parametric amplification experiment. . . . .   | 23 |
| 3.2  | Principal refractive indices for BBO crystal. . . . .   | 24 |
| 3.3  | Phase matching curve for second harmonic generation in a type-I BBO crystal. . . . .  | 25 |
| 3.4  | Phase matching curve for second harmonic generation in a type-II BBO crystal. . . . .   | 25 |
| 3.5  | Experimental setup for second harmonic generation. . . . .  | 27 |
| 3.6  | Average power of the second harmonic as a function of the average power of the fundamental at the input of the crystal when the focal length of L1 is 1 cm. . . . .       | 29 |
| 3.7  | Average power of the second harmonic as a function of the average power of the fundamental at the input of the crystal when the focal length of L1 is 2.5 cm. . . . .     | 29 |
| 3.8  | Average power of the second harmonic as a function of the average power of the fundamental at the input of the crystal when the focal length of L1 is 5 cm. . . . .       | 30 |
| 3.9  | Generation of the pump beam using focused Gaussian beams and a type-I BBO crystal. . . . .  | 31 |
| 3.10 | Experimental setup for degenerate optical parametric amplification. . . . .   | 34 |
| 3.11 | Beam geometry within the BBO crystal (not to scale). . . . .  | 35 |
| 3.12 | Comparison of experimental results with the computer simulation. . . . .  | 36 |
| 3.13 | Amplification and deamplification response of degenerate optical parametric amplifier for different power levels of the signal. . . . .                                   | 37 |
| 3.14 | Ratio of the pump power at the output to the pump power at the input for degenerate optical parametric amplifier for amplification and deamplification responses. . . . . | 37 |

|      |   |    |
|------|---|----|
| 3.15 | Experimental setup for nondegenerate optical parametric amplification. . . . .  | 39 |
| 3.16 | Parametric gain of nondegenerate optical parametric amplifier as a function of average power of the pump beam. The signal and the pump beams have the same polarization. . . . .    | 40 |
| 3.17 | Parametric gain of nondegenerate optical parametric amplifier as a function of average power of the pump beam. The signal and the pump beams have orthogonal polarizations. . . . . | 41 |

# Chapter 1

## INTRODUCTION

Optical properties of most materials are modified by the presence of intense light. Usually, the response of the material to the optical field is a nonlinear function of optical intensity. Nonlinear optics is the study of phenomena that occur as a consequence of this property of optical materials. Typically, with ordinary light sources, one cannot reach the intensity levels that are high enough to observe nonlinear effects. Only laser light is sufficiently intense to modify the optical properties of a material system by a discernible amount.

Experiments in nonlinear optics began right after the invention of the laser [1]. The first experiment in nonlinear optics was performed by Franken [2], where the frequency of a ruby laser was doubled using a quartz crystal as the nonlinear medium. In frequency doubling two photons at the same frequency combine to produce one photon at twice that frequency. Frequency doubling is one example of a broader class of nonlinear processes called three-wave mixing. Many experiments have been performed since then to demonstrate mixing of three optical waves. Other three-wave mixing processes are sum frequency generation, where two photons at different frequencies are combined to produce one photon at the sum frequency, and difference frequency generation, where one photon is split into two photons at lower frequencies. Theoretical analysis of difference frequency generation has shown that amplification of light waves in a second-order nonlinear medium is possible. This process, called optical parametric amplification, was first demonstrated by Wang and Racette [3] in 1965. Since then, parametric amplification has widely been investigated as an alternative to laser amplification.

The high optical intensities required to observe nonlinear effects are hard to attain with continuous wave (cw) lasers. The advent of pulsed lasers has solved this problem by providing very high intensities for a short duration of time. Further developments in laser technology have led to the usage of ultrafast laser systems that have pulsewidths on the order of 1 ps or less. These developments have opened up new research areas in optics.

Another important technological advance is the production of new materials with higher nonlinearities. Nowadays, most widely used nonlinear optical crystals are potassium titanyl phosphate (KTP), beta-barium borate (BBO), and lithium triborate (LBO). These materials not only have high nonlinearities, but they are also broadly transparent and chemically stable. The usage of both pulsed lasers and these highly nonlinear crystals has made optical parametric amplification a fruitful research area in nonlinear optics.

The gain produced by parametric amplifiers can be used to construct optical oscillators. An optical parametric amplifier placed inside an optical cavity provides gain much like a laser medium does in lasers. This cavity, pumped by an external laser source is called an optical parametric oscillator (OPO). Using OPOs, frequency down-conversion of laser outputs has become possible. This has important technological consequences, since lasers operate at a limited number of wavelengths and OPOs can extend this range to longer wavelengths. Moreover, OPOs can be wavelength tuned whereas most lasers operate at a single wavelength. Furthermore, extension to shorter wavelengths is possible by frequency doubling with another crystal inside the cavity. Optical parametric oscillation was first demonstrated by Giordimane and Miller [4] in 1965. With the improvements in ultrafast laser systems, synchronously pumped optical parametric oscillators [5] have been developed to generate tunable femtosecond and picosecond pulses.

Another important aspect of optical parametric amplification is the possibility of generating non-classical optical fields. According to quantum theory, a laser operating well above threshold emits light in a quantum state called the coherent state [6]. For a coherent state, the number of photons over an observation period shows a Poisson distribution, which means that the variance of the photon number (quantum noise) is equal to the average number of photons. This sets a so called quantum limit to the minimum amount of noise that a classical optical field can have at best. After Yuen [7] theoretically showed the existence of squeezed states, it was discovered that these states can be generated using optical parametric amplifiers [8]. Squeezed states have reduced

quadrature amplitude noise compared to the coherent states, and provide detection below the quantum limit [9]. Another method to provide detection below the quantum limit is also introduced using the benefit of highly correlated output photon streams (twin beams) of OPAs. A noise reduction of more than 6 dB is possible using pulsed twin beams of light [10].

In this thesis, we designed and implemented femtosecond optical parametric amplifiers based on BBO crystals. We used a mode-locked Titanium:Sapphire laser as our source. First, the output of the laser was frequency doubled using a BBO crystal. The second harmonic was used to pump our optical parametric amplifiers. The remaining portion of the field at the fundamental frequency was used as the signal input to the amplifier after being attenuated. At the output of the amplifier a third field, called the idler, was generated whose frequency is equal to the difference of the pump and the signal frequencies, which is equal to the frequency of the signal for our case.

We implemented two different types of optical parametric amplifiers. When the idler and the signal were indistinguishable from each other, the gain of the optical parametric amplifier was dependent on the phase difference between the pump and the signal beams. This amplifier is called a phase sensitive amplifier. When the signal and the idler were distinguishable, due to their orthogonal polarizations, we observed that the gain of the optical parametric amplifier was independent of phase, resulting in a phase insensitive amplifier.

Chapter 2 presents the theoretical background for three wave mixing in second-order nonlinear media. In Chapter 3, properties of the laser and BBO crystals are described, the experimental work is presented, and . In this chapter, results are compared with computer simulations. Finally, remarks and conclusions are provided in Chapter 4.

## Chapter 2

# THEORY OF OPTICAL PARAMETRIC AMPLIFICATION

This chapter discusses optical nonlinearities, and how nonlinear materials can be used for three wave mixing. The coupled field equations that characterize three wave mixing and some special case solutions, such as optical parametric amplification and second harmonic generation, are presented next. Finally, phase matching considerations are discussed.

### 2.1 Nonlinear Materials

All optical materials have some nonlinearity. To observe nonlinear effects experimentally, the nonlinearity of the material and the driving field intensity must be high enough. Some materials, which have higher nonlinearities with respect to others, show nonlinear responses to driving fields with high intensities provided by lasers. These are referred to as nonlinear materials.

In a non-magnetic material, the constitutive relations can be written as [11]

$$\mathbf{D} = \epsilon_0 \mathbf{E} + \mathbf{P} \quad (2.1)$$

$$\mathbf{B} = \mu_0 \mathbf{H} \quad (2.2)$$



where  $\mu_0$  and  $\epsilon_0$  are permeability and permittivity of free space,  $\mathbf{E}$  and  $\mathbf{H}$  are the electric and magnetic fields,  $\mathbf{D}$  and  $\mathbf{B}$  are the electric and magnetic flux densities, and  $\mathbf{P}$  is the induced polarization, respectively. For linear materials, the polarization is related to the electric field by [11]

$$\mathbf{P} = \epsilon_0 \overline{\overline{\chi}}^{(1)} \cdot \mathbf{E} \quad (2.3)$$

where  $\overline{\overline{\chi}}^{(1)}$  is known as the linear susceptibility tensor. The product of this tensor with a vector is known as the tensor product. One can always choose a Cartesian coordinate system such that only the diagonal elements of this tensor are nonzero. The elements of this tensor can be frequency dependent, to account for dispersion in the material.

For nonlinear materials, the polarization can be expressed as a power series of the electric field as [11]

$$\begin{aligned} \mathbf{P} &= \epsilon_0 \overline{\overline{\chi}}^{(1)} \cdot \mathbf{E} + \epsilon_0 \mathbf{E} \cdot \overline{\overline{\overline{\chi}}}^{(2)} \cdot \mathbf{E} + \epsilon_0 \mathbf{E} \cdot (\mathbf{E} \cdot \overline{\overline{\overline{\chi}}}^{(3)} \cdot \mathbf{E}) + \text{h.o.t} \\ &= \mathbf{P}^{(1)} + \mathbf{P}^{(2)} + \mathbf{P}^{(3)} + \text{h.o.t.} \end{aligned} \quad (2.4)$$

where  $\overline{\overline{\overline{\chi}}}^{(2)}$  and  $\overline{\overline{\overline{\chi}}}^{(3)}$  are the second and third order nonlinear susceptibility tensors.  $P^{(1)}$  is called linear polarization and  $P^{(n)}$  is called  $n$ th order nonlinear polarization ( $n > 1$ ). Usually, the effect of the second-order nonlinearity is much greater than all of the higher order nonlinearities. Therefore, one can neglect the effect of higher order nonlinearities if the second-order nonlinearity is nonzero. In centrosymmetric materials, which have inversion symmetry, the elements of even order susceptibility tensors vanish, which means that the second-order susceptibility also vanishes. In such materials, only the third order nonlinear effect is dominant.

In the analysis of nonlinear interactions, it is convenient to express the electric and second-order nonlinear polarization field vectors as discrete sums of frequency components as

$$\mathbf{E}(\mathbf{r}, t) = \frac{1}{2} \sum_n \left[ \mathbf{E}_n(\mathbf{r}) e^{j\omega_n t} + \mathbf{E}_n^*(\mathbf{r}) e^{-j\omega_n t} \right] \quad (2.5)$$

$$\mathbf{P}^{(2)}(\mathbf{r}, t) = \frac{1}{2} \sum_n \left[ \mathbf{P}_n^{(2)}(\mathbf{r}) e^{j\omega_n t} + \mathbf{P}_n^{(2)*}(\mathbf{r}) e^{-j\omega_n t} \right]. \quad (2.6)$$

The summations are over positive frequency components. When these expressions are substituted into Equation 2.4, we find that the second-order nonlinear polarization can be written as

$$\mathbf{P}_q^{(2)}(\mathbf{r}) = \frac{1}{2} D \epsilon_0 \mathbf{E}_m(\mathbf{r}) \cdot \overline{\overline{\overline{\chi}}}^{(2)}(\omega_q = \omega_m + \omega_n) \cdot \mathbf{E}_n(\mathbf{r}) \quad (2.7)$$

where  $D$  is the number of distinct permutations of the applied frequencies  $\omega_m$  and  $\omega_n$  [11]. Since  $\mathbf{E}_m$  is associated with the time dependence  $e^{j\omega_m t}$  and  $\mathbf{E}_n$  is associated with the time dependence  $e^{j\omega_n t}$ , the second-order nonlinear polarization resulting from their product is at a frequency of  $\omega_m + \omega_n$ . Therefore,  $\chi^{(2)}$  is expressed as a function of these three frequency arguments where the first argument is always the sum of the other two. Similarly

$$\mathbf{P}_m^{(2)}(\mathbf{r}) = \frac{1}{2} D \epsilon_0 \mathbf{E}_q(\mathbf{r}) \cdot \chi^{(2)}(\omega_m = \omega_q - \omega_n) \cdot \mathbf{E}_n^*(\mathbf{r}) \quad (2.8)$$

$$\mathbf{P}_n^{(2)}(\mathbf{r}) = \frac{1}{2} D \epsilon_0 \mathbf{E}_q(\mathbf{r}) \cdot \chi^{(2)}(\omega_n = \omega_q - \omega_m) \cdot \mathbf{E}_m^*(\mathbf{r}). \quad (2.9)$$

The reason for why the nonlinear polarization plays an important role is that a time varying polarization can act as the source of new components of the electromagnetic field. Equations (2.7), (2.8), and (2.9) show the existence of coupling between the fields at frequencies  $\omega_m$ ,  $\omega_n$ , and  $\omega_q$  ( $\omega_m + \omega_n = \omega_q$ ) in second-order nonlinear medium. This fact implies that three wave mixing is possible in second-order nonlinear medium. In the following section, we will describe how second-order nonlinearity can be used for three wave mixing.

## 2.2 Three Wave Mixing in Second-Order Nonlinear Materials

Maxwell's equations in a material where no free currents or charges are present can be written as

$$\nabla \cdot \mathbf{D} = 0 \quad (2.10)$$

$$\nabla \times \mathbf{E} = -\frac{\partial \mathbf{B}}{\partial t} \quad (2.11)$$

$$\nabla \cdot \mathbf{B} = 0 \quad (2.12)$$

$$\nabla \times \mathbf{H} = \frac{\partial \mathbf{D}}{\partial t}. \quad (2.13)$$

Using Equations (2.1) and (2.2) one can derive the wave equation as

$$\nabla \times \nabla \times \mathbf{E}(\mathbf{r}, t) + \frac{1}{c^2} \frac{\partial^2}{\partial t^2} \mathbf{E}(\mathbf{r}, t) = -\mu_0 \frac{\partial^2}{\partial t^2} \mathbf{P}(\mathbf{r}, t) \quad (2.14)$$

where  $\mathbf{P}(\mathbf{r}, t)$  is defined in Equation (2.4). Since we are considering materials that exhibit second-order nonlinearities, we ignore all higher order terms. We

further say that

$$\nabla \cdot \mathbf{E} = 0, \quad (2.15)$$

which is a direct consequence of Equation (2.10) in homogeneous media. Using Equation (2.15), writing the polarization as the sum of linear and nonlinear parts, and replacing  $(1 + \bar{\chi}^{(1)})$  with  $n^2$ , we end up with the equation

$$\nabla^2 \mathbf{E}(\mathbf{r}, t) - \frac{n^2}{c^2} \frac{\partial^2}{\partial t^2} \mathbf{E}(\mathbf{r}, t) = -\mu_0 \frac{\partial^2}{\partial t^2} \mathbf{P}^{(2)}(\mathbf{r}, t) \quad (2.16)$$

where we have used the vector identity  $\nabla \times \nabla \times \mathbf{E} = \nabla(\nabla \cdot \mathbf{E}) - \nabla^2 \mathbf{E}$ . Replacing  $(1 + \bar{\chi}^{(1)})$  with  $n^2$  is exactly true for isotropic materials. For anisotropic materials, this assumption is still valid if the propagation is along one of the principal axes, but otherwise fails since  $\mathbf{D}$  and  $\mathbf{E}$  vectors are no longer parallel to each other. This is known as the walk-off effect in birefringent materials. If we assume that walk-off is small and does not destroy the nature of three wave mixing in the length of the interaction, we can think of  $n$  as the effective refractive index seen by the electric field at that specific polarization.

For plane waves at frequencies  $\omega_1, \omega_2, \omega_3$  ( $\omega_3 = \omega_1 + \omega_2$ ) propagating along the  $z$ -axis we can write

$$\begin{aligned} \mathbf{E}_i(\mathbf{r}, t) &= \text{Re} \left[ \mathbf{E}_i(z) e^{j\omega_i t} \right] \\ &= \text{Re} \left[ \mathbf{A}_i(z) e^{j(\omega_i t - k_i z)} \right] \end{aligned} \quad (2.17)$$

$$\mathbf{P}_i^{(2)}(\mathbf{r}, t) = \text{Re} \left[ \mathbf{P}_i^{(2)}(z) e^{j(\omega_i t - k_i z)} \right] \quad (2.18)$$

where  $i = 1, 2, 3$ . Now we can write the wave equation in Fourier domain as

$$\nabla^2 (\mathbf{A}_3(z) e^{-jk_3 z}) + \frac{n_3^2 \omega_3^2}{c^2} \mathbf{A}_3(z) e^{-jk_3 z} = -\mu_0 \omega_3^2 \mathbf{P}_3^{(2)}(z). \quad (2.19)$$

Using Equation (2.7)  $\mathbf{P}_3^{(2)}(z)$  can be written as

$$\mathbf{P}_3^{(2)}(z) = \epsilon_0 \mathbf{E}_1(z) \cdot \bar{\chi}^{(2)}(\omega_3 = \omega_1 + \omega_2) \cdot \mathbf{E}_2(z). \quad (2.20)$$

Substituting

$$\begin{aligned} \mathbf{A}_i(z) &= A_i(z) \mathbf{a}_i \quad (2.21) \\ \nabla^2 A_3(z) e^{-jk_3 z} &= \frac{d^2}{dz^2} A_3(z) e^{-jk_3 z} \\ &= \frac{d^2 A_3(z)}{dz^2} e^{-jk_3 z} - 2jk_3 \frac{dA_3(z)}{dz} e^{-jk_3 z} \\ &\quad - k_3^2 A_3(z) e^{-jk_3 z} \end{aligned} \quad (2.22)$$

where  $\mathbf{a}_i$  is the unit vector in the direction of  $\mathbf{A}_i$ , and using the slowly varying envelope approximation [11]

$$\left| \frac{d^2 A_3(z)}{dz^2} \right| \ll \left| k_3 \frac{dA_3(z)}{dz} \right| \quad (2.23)$$

we end up with the equation

$$\begin{aligned} \frac{dA_3(z)}{dz} &= -j \frac{\mu_0 \omega_3^2}{2k_3} \mathbf{a}_3 \cdot \mathbf{P}_3^{(2)}(z) \\ &= -j \frac{\omega_3 d_3}{n_3 c} A_1(z) A_2(z) e^{-j\Delta k z} \end{aligned} \quad (2.24)$$

where

$$\Delta k = k_1 + k_2 - k_3 \quad (2.25)$$

is the phase mismatch per unit length, and

$$d_3 = \frac{1}{2} \mathbf{a}_3 \cdot (\mathbf{a}_1 \cdot \overline{\overline{\chi}}^{(2)}(\omega_3 = \omega_1 + \omega_2) \cdot \mathbf{a}_2) \quad (2.26)$$

is the effective second-order nonlinear coefficient. Similarly, for fields at  $\omega_1$  and  $\omega_2$  we get

$$\frac{dA_1(z)}{dz} = -j \frac{\omega_1 d_1}{n_1 c} A_2^*(z) A_3(z) e^{j\Delta k z} \quad (2.27)$$

$$\frac{dA_2(z)}{dz} = -j \frac{\omega_2 d_2}{n_2 c} A_1^*(z) A_3(z) e^{j\Delta k z} \quad (2.28)$$

where

$$d_1 = \frac{1}{2} \mathbf{a}_1 \cdot (\mathbf{a}_2 \cdot \overline{\overline{\chi}}^{(2)}(\omega_1 = -\omega_2 + \omega_3) \cdot \mathbf{a}_3) \quad (2.29)$$

$$d_2 = \frac{1}{2} \mathbf{a}_2 \cdot (\mathbf{a}_3 \cdot \overline{\overline{\chi}}^{(2)}(\omega_2 = \omega_3 - \omega_1) \cdot \mathbf{a}_1). \quad (2.30)$$

In a lossless medium, permutation symmetry requires [11]

$$d_1 = d_2 = d_3 = d = d^*. \quad (2.31)$$

Equations (2.24), (2.27), and (2.28) describe the interaction of three collinear plane waves in a  $\overline{\overline{\chi}}^{(2)}$  medium under the slowly varying amplitude approximation. The general solutions to  $A_1$ ,  $A_2$ , and  $A_3$  are in terms of Jacobi elliptic functions [12]. Given the field amplitudes at the input plane ( $z = 0$ ) of a nonlinear material, these general solutions can be used to calculate field amplitudes at the output plane ( $z = L$ ). The initial values are important since they determine the type of nonlinear interaction.

Possible types of nonlinear interactions in second-order nonlinear medium are sum frequency generation (SFG), difference frequency generation (DFG),

and second harmonic generation (SHG). In SFG, the fields at two different frequencies,  $\omega_1$  and  $\omega_2$ , are combined to produce an output at the sum frequency  $\omega_3 = \omega_1 + \omega_2$ . SHG is the degenerate case of SFG in which the two input fields have the same frequency. As a result, a field twice at the input frequency is present at the output. In DFG, the fields at two different frequencies,  $\omega_3$  and  $\omega_1$ , are combined to produce an output at the difference frequency  $\omega_2 = \omega_3 - \omega_1$ . The theoretical analysis of DFG shows that the field at  $\omega_1$  is amplified during the process. Therefore, DFG is also called optical parametric amplification.

In this thesis we restrict ourselves to optical parametric amplification and second harmonic generation cases only. The reason for why second harmonic generation is investigated is that it is used as a pump source for our optical parametric amplifier experiments.

## 2.3 Nondegenerate Optical Parametric Amplification

Optical parametric amplification is the process where the frequencies  $\omega_1$  and  $\omega_3$  are mixed to produce the difference frequency  $\omega_2 = \omega_3 - \omega_1$ . In this interaction, the photons at frequency  $\omega_3$  are split into photons at frequencies  $\omega_1$  and  $\omega_2$  accounting for an increase in the number of photons at frequency  $\omega_1$ . As a result, the intensity of the field at  $\omega_1$  is amplified and photons at frequency  $\omega_2$  are created. The field at frequency  $\omega_3$  is called the pump since it is the energy source for the fields at the other two frequencies. The field at frequency  $\omega_1$  is called the signal since it is the amplified field and the field at frequency  $\omega_2$  is called the idler.

The signal and idler fields may be distinguished from each other by their frequencies, polarizations, or directions of propagation. If all these properties are the same, then the signal and idler are indistinguishable from each other. This situation is referred to as the degenerate case. If at least one of the properties is different, then the signal and idler fields are distinguishable, and the interaction is nondegenerate. Figure 2.1 shows the schematic and energy diagram for optical parametric amplification.

We use the subscripts  $s$ ,  $i$ , and  $p$  instead of 1, 2, 3 to represent the signal, idler, and pump waves. Putting the initial conditions such that the pump field

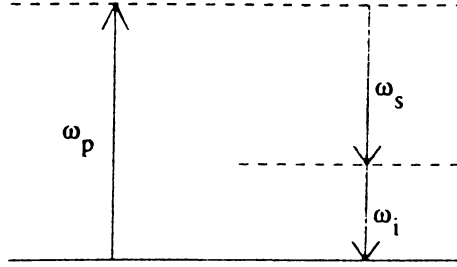
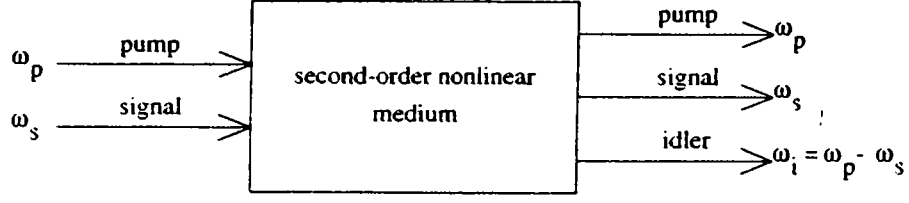


Figure 2.1: Schematic and energy diagram for optical parametric amplification. The dashed lines are virtual states.

is much stronger with respect to the signal and idler fields, i.e.  $A_p$  is assumed not to be depleted during the interaction and stays constant, the coupled mode equations become

$$\frac{dA_s(z)}{dz} = -j \frac{\omega_s d}{n_s c} A_i^*(z) A_p e^{j\Delta k z} \quad (2.32)$$

$$\frac{dA_i(z)}{dz} = -j \frac{\omega_i d}{n_i c} A_s^*(z) A_p e^{j\Delta k z}. \quad (2.33)$$

For  $\Delta k = 0$ , which is referred to as the phase matched case, the solution to these equations can be written as [13]

$$A_s(z) = A_s(0) \cosh(\kappa z) - j e^{j\phi_p} \sqrt{\frac{n_i \omega_s}{n_s \omega_i}} A_i^*(0) \sinh(\kappa z) \quad (2.34)$$

$$A_i(z) = A_i(0) \cosh(\kappa z) - j e^{j\phi_p} \sqrt{\frac{n_s \omega_i}{n_i \omega_s}} A_s^*(0) \sinh(\kappa z) \quad (2.35)$$

where  $\phi_p$  is the pump phase, i.e.,  $A_p = |A_p| e^{j\phi_p}$ . The value of  $\kappa$  is

$$\kappa^2 = \frac{2\omega_s \omega_i d^2 I_p}{\epsilon_0 n_s n_i n_p c^3} \quad (2.36)$$

where  $I_p$  is the intensity of the pump beam which is related to the amplitude of the electric field by

$$I_p = \frac{1}{2} n_p \epsilon_0 c |A_p|^2. \quad (2.37)$$

Since the input idler field is zero ( $A_i(0) = 0$ ), the solutions become

$$A_s(z) = A_s(0) \cosh(\kappa z) \quad (2.38)$$

$$A_i(z) = -j e^{j\phi_p} \sqrt{\frac{n_s \omega_i}{n_i \omega_s}} A_s^*(0) \sinh(\kappa z). \quad (2.39)$$

The parametric gain  $g$  for a medium of length  $L$  is defined as

$$g \equiv \left| \frac{A_s(L)}{A_s(0)} \right|^2 = \cosh^2(\kappa L). \quad (2.40)$$

The gain for the idler wave is

$$g' \equiv \frac{I_i(L)}{I_s(0)} = \frac{n_i}{n_s} \left| \frac{A_i(L)}{A_s(0)} \right|^2 = \frac{\omega_i}{\omega_s} \sinh^2(\kappa L). \quad (2.41)$$

These solutions show us the phase insensitive nature of the nondegenerate optical parametric amplifier. The field phases depend on the pump phase, but the intensity of the signal and the idler beams do not. Because of this independence, this amplifier is sometimes called a phase insensitive amplifier.

Figure 2.2 shows the evolution of the signal and idler intensities for a nondegenerate optical parametric amplifier. The signal and the idler are assumed to have the same frequency ( $\omega_i = \omega_s$ ) but still nondegenerate (due to polarizations). The signal intensity, (hence the parametric gain) is a monotonically increasing function of crystal length. Figure 2.3 shows how the parametric gain depends on the pump intensity. The parametric gain is a monotonically

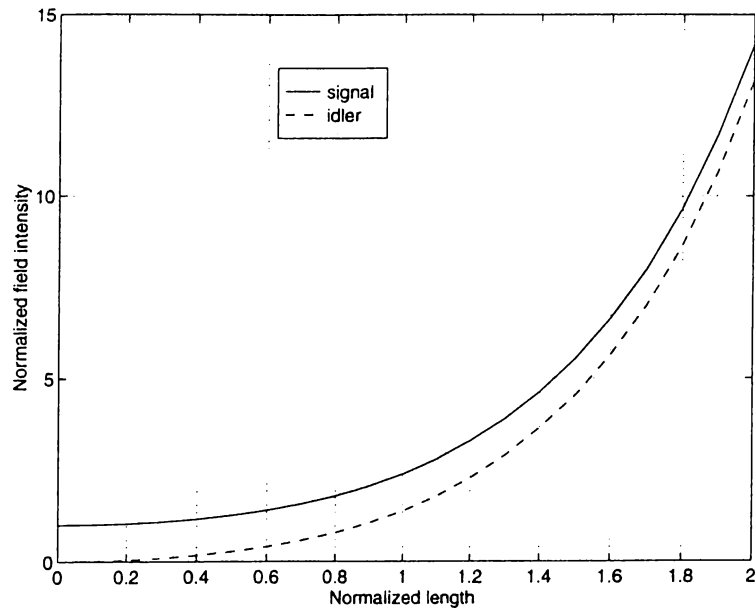


Figure 2.2: Spatial evolution of signal and idler field intensities for a nondegenerate optical parametric amplifier for the case of no phase mismatch in the constant pump approximation. The horizontal axis is normalized with respect to  $\kappa^{-1}$  and the vertical axis is normalized with respect to the intensity of the signal at  $z = 0$ .

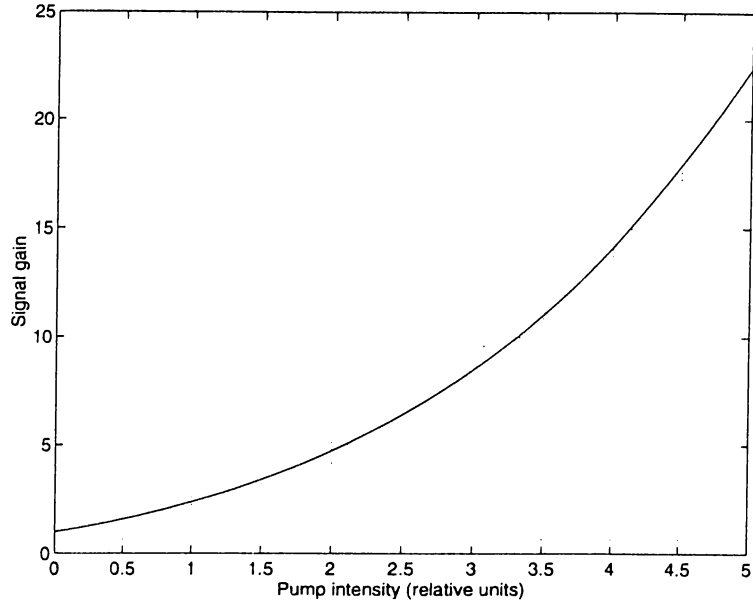


Figure 2.3: Dependence of parametric gain on the pump field intensity for constant length of interaction. The horizontal axis is normalized with respect to the value of the pump intensity satisfying  $\kappa L = 1$ .

increasing function of the pump intensity. One can expect this since nonlinear effect is more efficient for higher pump intensities.

When the interaction is not phase matched, i.e.  $\Delta k \neq 0$ , the signal gain is modified to [13]

$$g = \cosh^2(\kappa' L) \quad (2.42)$$

where

$$\kappa'^2 = \kappa^2 - \left(\frac{\Delta k}{2}\right)^2 \quad (2.43)$$

for the range  $|\Delta k L| < 2$ , under the assumption of a strong pump beam. Figure 2.4 shows the signal gain as a function of the phase mismatch for  $\kappa = 1000 \text{ m}^{-1}$  and  $L = 1 \text{ mm}$ . For nonzero  $\Delta k$  a decrease in the signal gain is introduced which states that the nonlinear effect in question is less efficient. This fact is not only true for optical parametric amplification, but also for other types of nonlinear interactions (SFG, DFG, and SHG). For all types of nonlinear interactions  $\Delta k = 0$  has to be satisfied for efficient generation of the fields [11].

The solutions up to now describe the evolution of the fields under the assumption of an undepleted pump field. More general solutions, that take pump depletion into account, are in terms of Jacobi elliptic functions. Under the assumption of undepleted pump field, these functions reduce to the solutions



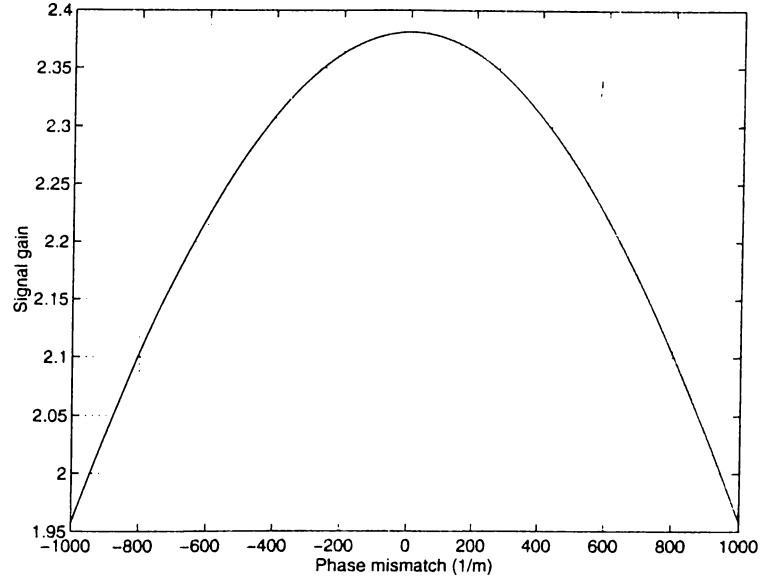


Figure 2.4: The signal gain of a nondegenerate optical parametric amplifier as a function of  $\Delta k$ . The gain has a maximum where  $\Delta k = 0$ .

given here [12]. If we extend the length of the interaction or the pump intensity, we can no longer assume that the pump is not depleted since for every photon created at the signal frequency, a photon at the pump frequency is annihilated. As a result, the field intensity of the pump decreases as the interaction goes on, and when all the pump photons are annihilated the field intensities of the signal and the idler reaches to a maximum. Figure 2.5 shows the exact solution of the coupled wave equations. The photon flux of the signal at the input is  $1/500$  of the photon flux of the pump and the photon flux of the idler at the input is zero. The relation between the photon flux and intensity is

$$\Phi = \frac{I}{\hbar\omega} \quad (2.44)$$

and the normalization length is given by

$$\kappa^{-1} = \sqrt{\frac{\epsilon_0 n_s n_i n_p c^3}{2\omega_s \omega_i d^2 I_p(0)}}. \quad (2.45)$$

The figure shows that when the pump begins to get depleted, the gain for the signal and the idler begin to saturate. When the pump photon flux is zero, all of the pump is converted to signal and idler frequencies. After this point back conversion starts and signal and idler photons combine to produce pump photons.

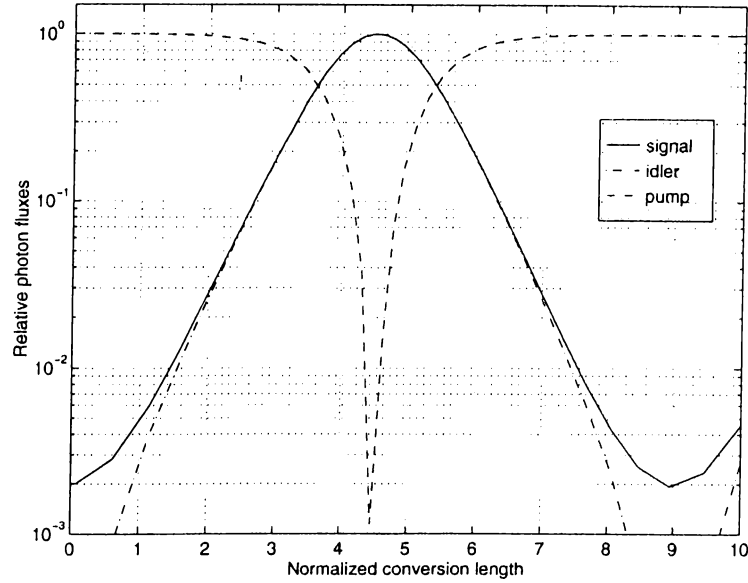


Figure 2.5: Spatial evolution of signal and idler and pump photon fluxes for nondegenerate optical parametric amplifier for the case of no phase mismatch. The horizontal axis is normalized with respect to  $\kappa^{-1}$  and the vertical axis is normalized with respect to the photon flux density of the pump at the input.

## 2.4 Degenerate Optical Parametric Amplification

In degenerate optical parametric amplification the signal and idler beams are indistinguishable, having the same frequency, polarization, and propagation direction. Substituting  $\omega_p = 2\omega$  and  $\omega_s = \omega_i = \omega$ , Equations (2.32) and (2.33) reduce to

$$\frac{dA_\omega(z)}{dz} = -j \frac{2\omega d}{n_\omega c} A_\omega^*(z) A_{2\omega} e^{j\Delta k z} \quad (2.46)$$

where

$$\Delta k = k_{2\omega} - 2k_\omega \quad (2.47)$$

under the assumption of a strong pump beam. For the phase matched case the solution to this equation is given by [13]

$$A_\omega(z) = A_\omega(0) \cosh(\kappa z) - j e^{j\phi_{2\omega}} A_\omega^*(0) \sinh(\kappa z) \quad (2.48)$$

where  $A_{2\omega} = |A_{2\omega}| e^{j\phi_{2\omega}}$  and

$$\kappa^2 = \frac{2\omega^2 d^2 I_{2\omega}}{\epsilon_0 n_\omega^2 n_{2\omega} c^3}. \quad (2.49)$$

Since phase is relative, we can arbitrarily choose the phase of one of the fields. If we choose the phase of the signal to be zero, i.e.  $A_\omega(0)$  is real, then the pump phase is also the phase difference between pump and the signal. The intensity of the signal can be written as

$$I_\omega(z) = \frac{1}{2} n_s \epsilon_0 c |A_\omega(0)|^2 |\cosh(\kappa z) - j e^{j\phi_{2\omega}} \sinh(\kappa z)|^2. \quad (2.50)$$

This amplifier is sometimes called a phase sensitive amplifier since the output field intensity of the signal depends on the phase between the pump and the signal beams. As a result, the parametric gain is also phase dependent and can be written as

$$g \equiv \left| \frac{A_\omega(L)}{A_\omega(0)} \right|^2 = |\cosh(\kappa L) - j e^{j\phi_{2\omega}} \sinh(\kappa L)|^2. \quad (2.51)$$

The gain curve reaches to a maximum and minimum at  $\phi_{2\omega} = \pi/2$  and  $\phi_{2\omega} = -\pi/2$ , respectively. For  $\phi_{2\omega} = \pm\pi/2$  the gain is calculated to be

$$g = e^{\pm 2\kappa L}. \quad (2.52)$$

Figure 2.6 shows the response of phase sensitive and insensitive optical parametric amplifiers for the same value of  $\kappa L$ . The maximum gain that the phase sensitive amplifier can reach is greater than that of the phase insensitive amplifier. The product of the maximum and minimum gain is always unity. Because of the phase sensitive nature of the amplifier the response is not always amplification. The gain curve always has a region below unity which means that the signal is deamplified at this point.

Equation 2.46 describes the evolution of the signal field in degenerate optical parametric amplification under the assumption that the pump is much stronger than the signal, i.e. stays constant during the interaction. When the field intensities of the pump and the signal are comparable this equation is no longer valid. For the amplification case, photons at the pump frequency are annihilated to create photons at the signal frequency accounting for a decrease at the pump field. As a result the gain begins to saturate just like it does in the case of the nondegenerate optical parametric amplifier. For the deamplification case, however, the photons at the signal frequency combine to create photons at the pump frequency accounting for an increase in the pump field. As a result, the pump field increases and the deamplification is enhanced.

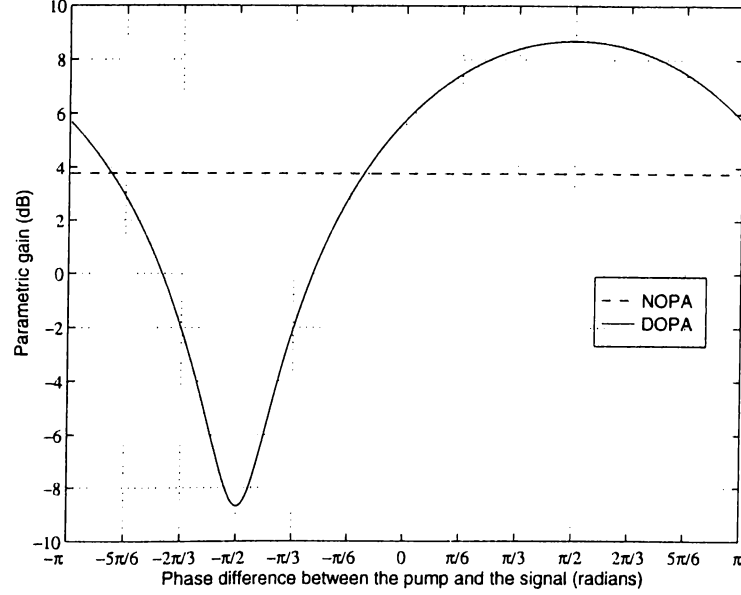


Figure 2.6: Parametric gain of nondegenerate optical parametric amplifier (NOPA) and degenerate optical parametric amplifier (DOPA) when  $\kappa L = 1$  as a function of phase difference between the pump and the signal.

## 2.5 Second Harmonic Generation

Second harmonic generation is a special case of three wave mixing where the photons at frequency  $\omega$  are mixed with themselves to generate photons at frequency  $2\omega$ . The differential equations for second harmonic generation are the same as the equations for degenerate optical parametric amplification except for the initial conditions. In second harmonic generation, the aim is to convert the field at  $\omega$  to the field at  $2\omega$ , i.e. we want to deplete the field at  $\omega$  and create a field at  $2\omega$ . For this reason, we can no longer neglect the  $z$  variation of any of the beams, i.e. none of the fields are constant. Figure 2.7 shows the schematic and energy diagram for second harmonic generation.

The coupled equations for second harmonic generation are

$$\frac{dA_{\omega}(z)}{dz} = -j \frac{\omega d}{n_{\omega} c} A_{2\omega}(z) A_{\omega}^*(z) e^{j\Delta k z} \quad (2.53)$$

$$\frac{dA_{2\omega}(z)}{dz} = -j \frac{\omega d}{n_{2\omega} c} A_{\omega}^2(z) e^{-j\Delta k z} \quad (2.54)$$

where

$$\Delta k = 2k_{\omega} - k_{2\omega} \quad (2.55)$$

is the phase mismatch per unit length. Introducing the normalized length

$$\xi = z/l \quad (2.56)$$

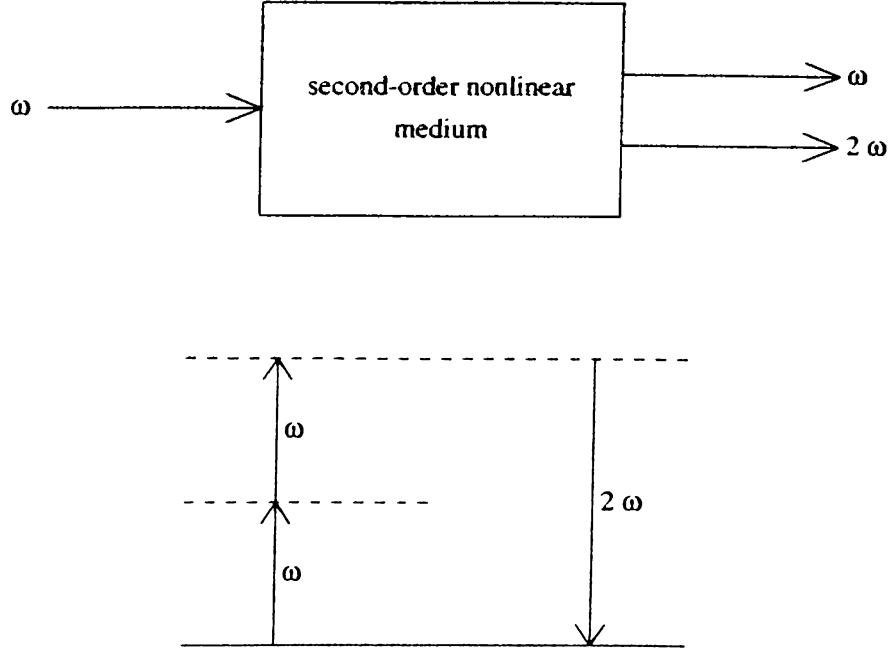


Figure 2.7: Schematic and energy diagram for second harmonic generation.

$$l = \sqrt{\frac{\epsilon_0 n_{2\omega} n_{\omega}^2 c^3}{2\omega^2 d^2 I_{\omega}(0)}} \quad (2.57)$$

and giving the initial condition  $A_{2\omega} = 0$  at the input, the amplitudes of the solutions to these coupled equations for the phase matched case can be given as [11]

$$|A_{\omega}(z)| = |A_{\omega}(0)| \operatorname{sech} \xi \quad (2.58)$$

$$|A_{2\omega}(z)| = |A_{\omega}(0)| \tanh \xi. \quad (2.59)$$

Figure 2.8 shows the spatial evolution of the fundamental and second-harmonic field intensities for the case of perfect phase matching and the boundary condition of no second harmonic field at the input. We see that when second harmonic field intensity at the input is zero, all of the incident radiation is converted to second harmonic in the limit  $\xi \rightarrow \infty$ . If the second harmonic field intensity at the input is not zero the evolution of intensities depends on the phase between the fundamental and second harmonic just like it does in the case of phase sensitive amplification [11]. This phase sensitive nature is expected since the coupled equations are the same for both.

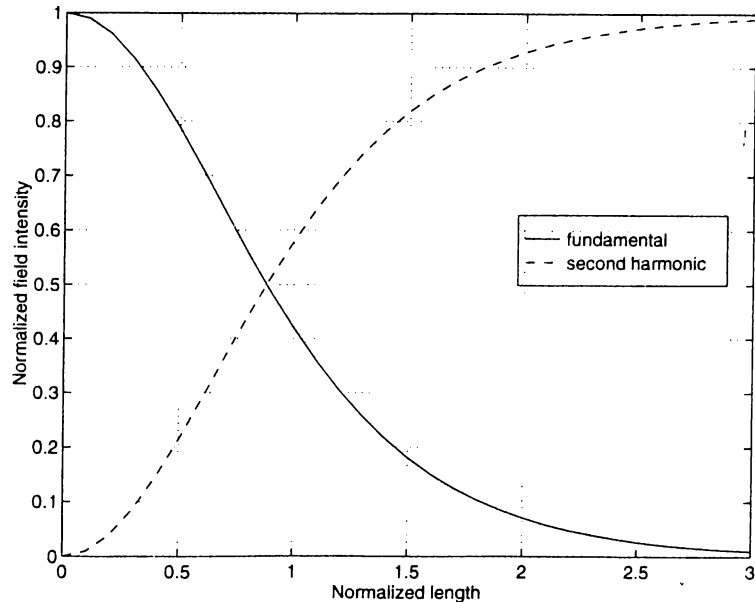


Figure 2.8: Spatial evolution of the fundamental and second harmonic field intensities for the case of perfect phase matching and the boundary condition of no second harmonic field at the input. The intensity is normalized with respect to the intensity of the fundamental at the input.

## 2.6 Phase Matching

In Section 2.3, it is said that the nonlinear effect in question is less efficient for nonzero  $\Delta k$  in all three wave interactions. To achieve  $\Delta k = 0$  the equations

$$n_1\omega_1 + n_2\omega_2 = n_3\omega_3 \quad (2.60)$$

$$\omega_1 + \omega_2 = \omega_3 \quad (2.61)$$

have to be satisfied simultaneously. For isotropic crystals this is impossible if the crystal has a refractive index that is a monotonic function of frequency within the band of interest. The most common way to achieve phase matching is to use birefringent crystals for which the refractive index is dependent on the polarization and the direction of propagation of optical field. Unlike isotropic crystals, we do not have a unique refractive index for an optical field with frequency  $\omega$ . In order to achieve phase-matching, the highest frequency wave  $\omega_3$  is polarized in the direction that gives it the lowest possible refractive index. There are two choices for the polarizations of the lower-frequency waves[14]. If the waves at frequencies  $\omega_1$  and  $\omega_2$  have the same polarization which is orthogonal to the polarization of the wave at frequency  $\omega_3$ , this is called type-I phase-matching. For type-II phase matching, the waves at frequencies  $\omega_1$  and  $\omega_2$  have orthogonal polarizations and one of them has the same polarization with the highest frequency wave  $\omega_3$ . Figure 2.9 shows the

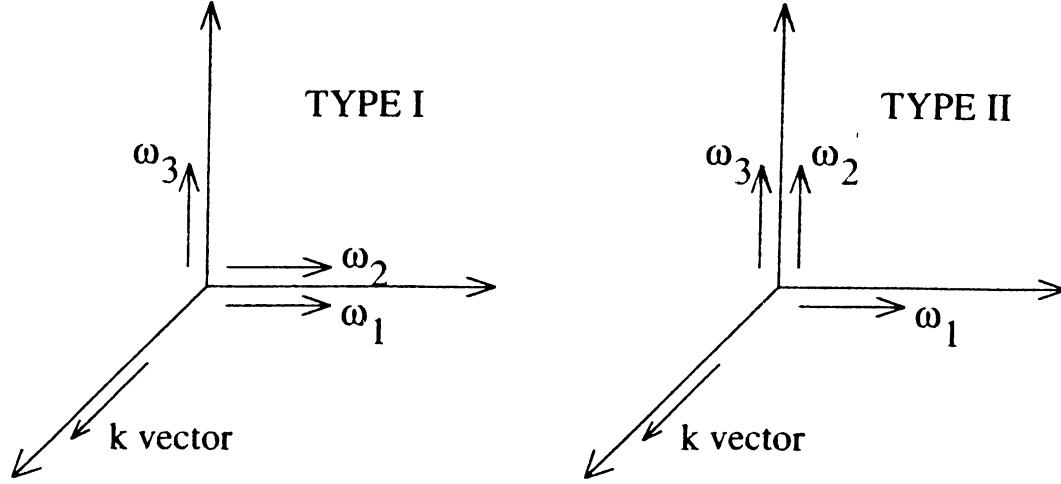


Figure 2.9: Directions of polarizations for  $\omega_1$ ,  $\omega_2$ , and  $\omega_3$  for type-I and type-II phase matching in three wave mixing ( $\omega_1 + \omega_2 = \omega_3$ ).

directions of polarization of the waves in type-I and type-II phase matching.

One can always choose a Cartesian coordinate system such that only the diagonal elements of the linear susceptibility tensor of the birefringent crystal are nonzero. This coordinate system defines the principal axes of the crystal. The nonzero elements of this tensor correspond to refractive indices

$$n_x = [1 + \chi_{xx}]^{1/2} \quad (2.62)$$

$$n_y = [1 + \chi_{yy}]^{1/2} \quad (2.63)$$

$$n_z = [1 + \chi_{zz}]^{1/2} \quad (2.64)$$

known as principal refractive indices. For the situation where

$$n_x \neq n_y \neq n_z \quad (2.65)$$

the crystal is said to be biaxial. By convention,  $x$ ,  $y$ ,  $z$  are the axes which satisfy

$$n_x < n_y < n_z. \quad (2.66)$$

If two of the indices are the same, the crystal is said to be uniaxial. For uniaxial crystals,  $x$ ,  $y$ ,  $z$  are the axes which satisfy

$$n_z \neq n_x = n_y \quad (2.67)$$

where  $z$ -axis is called the optic axis and  $n_x$  and  $n_y$  are called the ordinary refractive indices. If  $n_z < n_x$  then the crystal is called negative uniaxial whereas it is called positive uniaxial if  $n_z > n_x$ .

Since phase matching in our experiments is achieved using uniaxial crystals, in this section we will only deal with uniaxial crystals. In uniaxial crystals,

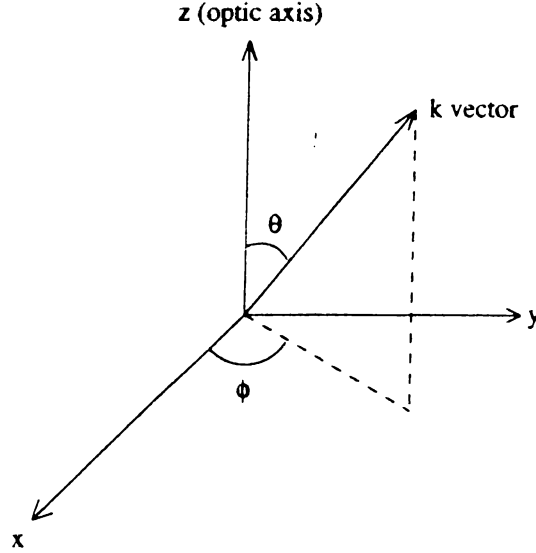


Figure 2.10:  $\theta$  and  $\phi$  angles defined due to spherical coordinates.

light polarized perpendicular to the plane containing the propagation vector  $\mathbf{k}$  and the optic axis is said to have the ordinary polarization. Such light experiences ordinary refractive index. Light polarized in the plane containing  $\mathbf{k}$  and the optic axis is said to have extraordinary polarization and experiences a refractive index  $n_e(\theta)$  that depends on the angle  $\theta$  between the optic axis and  $\mathbf{k}$  according to the relation

$$\frac{1}{n_e(\theta)^2} = \frac{\sin^2 \theta}{n_z^2} + \frac{\cos^2 \theta}{n_x^2}. \quad (2.68)$$

Figure 2.10 shows the  $\theta$  and  $\phi$  angles which are defined due to spherical coordinates.

According to the definitions of type-I and type-II phase-matchings, the field at frequency  $\omega_3$  must have lowest possible index. For negative uniaxial crystals this corresponds to extraordinary polarization and phase matching condition becomes

$$n_e(\omega_3, \theta)\omega_3 = n_x(\omega_1)\omega_1 + n_x(\omega_2)\omega_2 \quad (2.69)$$

for type-I. Similarly for type-II phase matching the condition is

$$n_e(\omega_3, \theta)\omega_3 = n_e(\omega_1, \theta)\omega_1 + n_x(\omega_2)\omega_2 \quad (2.70)$$

where  $\omega_1$  and  $\omega_2$  is interchangeable. For positive uniaxial crystals the field at frequency  $\omega_3$  have ordinary polarization. Phase matching conditions for positive uniaxial crystals are

$$n_x(\omega_3) = n_e(\omega_1, \theta)\omega_1 + n_e(\omega_2, \theta)\omega_2 \quad (2.71)$$

$$n_x(\omega_3) = n_x(\omega_1)\omega_1 + n_e(\omega_2, \theta)\omega_2 \quad (2.72)$$



for type-I and type-II, respectively.

The dependence of  $n_x$ ,  $n_y$ , and  $n_z$  on frequency are given by Sellmeier equations [14]. Using Sellmeier equations, Equations (2.69), (2.70), (2.71), and (2.72) can be solved numerically to give us a  $\theta$  angle corresponding to  $\omega_1$ ,  $\omega_2$ , and  $\omega_3$ . The angular orientation of the crystal should be adjusted precisely to this angle to achieve the phase matching condition. This method is widely used and is called angle tuning.

## Chapter 3

# EXPERIMENTAL WORK

All of the experiments based on nonlinear effects in optical materials depend on the intensity of the optical beams. The interaction strength usually increases with optical intensity. In Chapter 1, it was noted that pulsed lasers are ideal for reaching the high intensities required by these experiments. Recent experiments showed that optical parametric amplification can be achieved using Q-switched lasers whose pulse energies are in the order of 100 mJ and pulse durations in the order of 100 ns [12]. This yields a peak power level of 3 MW. That much of power focused to a spot size of  $30\ \mu\text{m}$  gives a peak intensity of  $10^{15}\ \text{W}/\text{m}^2$  which is high enough to achieve parametric conversion using typical nonlinear materials.

Our experiments that are described in this chapter are aimed at constructing and evaluating OPAs that are pumped by an ultrafast laser. The duration of pulses that are used in our experiments are in the order of 100 fs. In Sections 3.1 and 3.2 the properties of the laser source and the nonlinear crystals that we used are outlined. Our optical parametric amplifier (OPA) experiments and results are described in Section 3.4 together with comparisons with computer simulations.

Figure 3.1 shows a simplified schematic of our optical parametric amplifier experiments. We use a mode-locked Titanium:Sapphire laser as our ultrafast source. The output of this laser at a wavelength of 830 nm (infrared) is first frequency doubled to 415 nm (blue). The second harmonic is used as the pump of our optical parametric amplifier. The remaining portion of the field at the fundamental frequency is used as the signal input to the amplifier after

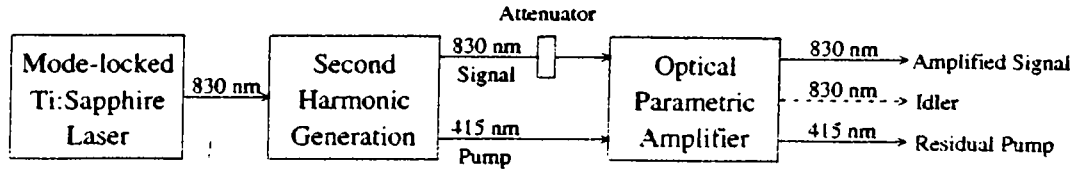


Figure 3.1: Schematic of the optical parametric amplification experiment.

being attenuated. For the degenerate OPA case, there are amplified signal and residual pump beams at the output of the amplifier, whereas an idler beam is also present at the output for the nondegenerate case.

### 3.1 The Laser

A mode-locked Titanium:Sapphire ( $\text{Ti:Al}_2\text{O}_3$ ) laser (Coherent model Mira-900F) is used in our experiments. The wavelength of the laser can be tuned in the 700-1000 nm range. The longitudinal modes of the laser are separated from each other by 76 MHz. Kerr-lens mode-locking is employed to achieve nearly transform limited pulses of approximately 120 fs at a repetition rate of 76 MHz.

There are two phenomena which affect pulse shaping in the Ti:Sapphire laser, namely group velocity dispersion (GVD) and self phase modulation (SPM). Contributions to the total GVD of the laser cavity arise from all optical components. These have positive GVD creating a frequency chirp on the pulse where the red frequency components travel faster than the blue. SPM is a result of intensity dependent refractive index, which is caused by the third-order nonlinearity in Ti:Sapphire crystal. Nearly transform limited soliton-like pulses occur if these opposite chirp contributions cancel each other on each round trip in the laser cavity. In Mira-900F the amount of SPM is not enough to compensate positive GVD by itself, therefore a reduction of positive GVD is necessary. Mira-900F has an intracavity prism pair designed to provide the necessary negative GVD. Introducing different amounts of negative GVD into the cavity, nearly transform limited, quasi-soliton pulses in the 100-200 fs range can be obtained.

Since high peak power is important in our experiments, we adjust the wavelength of the laser to 830 nm at which the laser output power reaches a maximum. At this wavelength the output of the laser is 800 mW resulting in an instantaneous peak power of 75 KW. We measure the duration of our

laser pulses with an autocorrelator (Femtochrome model FR103XL). At this wavelength we measured the autocorrelation of our pulses to be 210 fs. When deconvolved assuming a hyperbolic secant pulse shape, the pulse duration is deduced to be 140 fs.

## 3.2 Beta-Barium Borate Crystal

Beta-Barium Borate ( $\beta - \text{Ba}_2\text{BO}_4$ ) is a  $3m$  point group [14] negative uniaxial crystal whose transparency range is between  $0.198 - 2.6 \mu\text{m}$ . The Sellmeier equations describing the dispersion relations for  $n_z$  and  $n_x$  can be written as[14]

$$n_x^2 = 2.7045 + \frac{0.0184}{\lambda^2 - 0.0179} - 0.0155\lambda^2 \quad (3.1)$$

$$n_z^2 = 2.3730 + \frac{0.0128}{\lambda^2 - 0.0156} - 0.0044\lambda^2. \quad (3.2)$$

Figure 3.2 shows the principal indices for beta-barium borate (BBO) crystal. Since BBO is a negative uniaxial crystal  $n_z$  is always smaller than  $n_x$ .

The phase matching angle  $\theta$  for the BBO crystal can be found using Equations (2.69), (2.70), (3.1), and (3.2) for type-I and type-II phase matching for various wavelengths (See Section 2.6). Figure 3.3 and Figure 3.4 show the phase matching angles for second harmonic generation in type-I and type-II

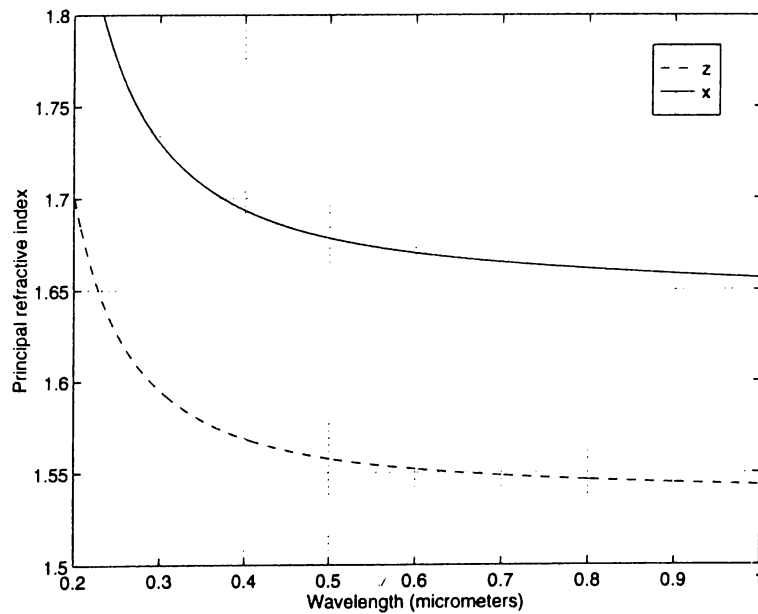


Figure 3.2: Principal refractive indices for BBO crystal.

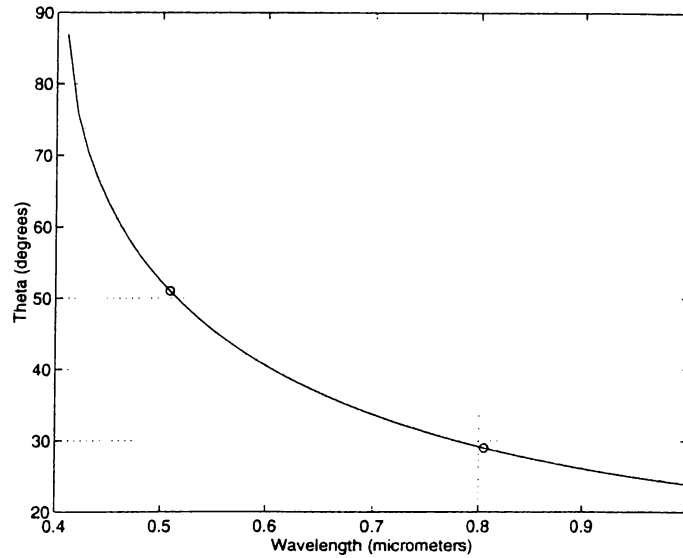


Figure 3.3: Phase matching curve for second harmonic generation in a type-I BBO crystal. The horizontal axis shows the wavelength of the fundamental beam in  $\mu\text{m}$  and the vertical axis shows the value of  $\theta$  in degrees.

BBO crystals, respectively, both as functions of the wavelength of the fundamental. Although these angles are calculated for second harmonic generation, they are also valid for our degenerate and nondegenerate optical parametric amplification experiments, since the idler and the signal field has twice the wavelength of the pump field. For these configurations, the horizontal axis is the wavelength of the signal.

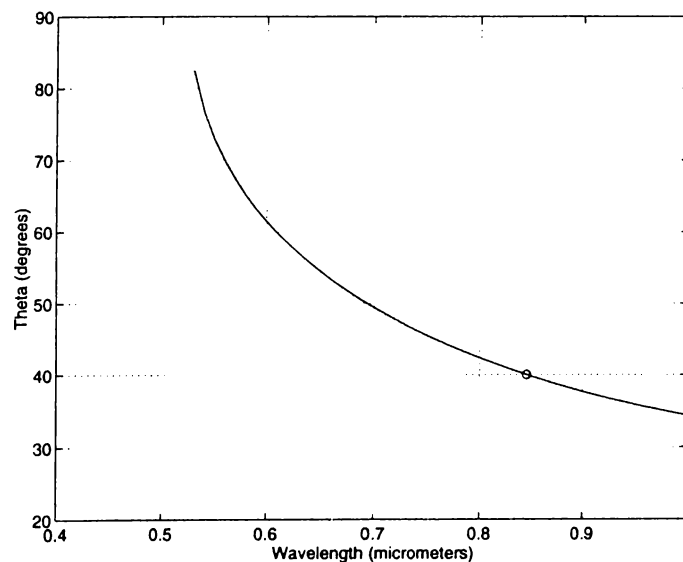


Figure 3.4: Phase matching curve for second harmonic generation in a type-II BBO crystal. The horizontal axis shows the wavelength of the fundamental beam in  $\mu\text{m}$  and the vertical axis shows the value of  $\theta$  in degrees.

Figure 3.3 and Figure 3.4 show that the entire range of the Ti:Sapphire laser can be frequency doubled using both type-I and type-II BBO crystals. This also implies that all of the range of the Ti:Sapphire laser can be used as the signal input to BBO based optical parametric amplifiers if the frequency doubled output of the laser is used as the pump beam.

The effective nonlinear coefficient of the BBO crystal at any  $\theta$  and  $\phi$  angle (See Figure 2.10) can be calculated using Equation (2.26). The effective nonlinear coefficient is dependent on the polarizations of the three waves and also on the direction of propagation. For  $3m$  point group crystals, this coefficient is calculated to be [14]

$$d = d_{31} \sin \theta - d_{22} \cos \theta \sin 3\phi \quad (3.3)$$

for type-I and

$$d = d_{22} \cos^2 \theta \cos 3\phi \quad (3.4)$$

for type-II phase matching. For the BBO crystal  $d_{31}$  and  $d_{22}$  are [14]

$$d_{31} = \frac{1}{2} \chi_{zxx} = 0.12 \times 10^{-12} \text{ m/V} \quad (3.5)$$

$$d_{22} = \frac{1}{2} \chi_{yyy} = 1.78 \times 10^{-12} \text{ m/V}. \quad (3.6)$$

The value of  $\theta$  is calculated from the phase matching condition whereas the value of  $\phi$  is chosen to maximize the effective nonlinear coefficient. The optimum value of  $\phi$  is  $90^\circ$  for type-I phase matching whereas it is  $0^\circ$  or  $60^\circ$  for type-II phase matching, independent of the wavelength.

Three BBO crystals are used during the experiments. The wavelengths corresponding to these crystals are pointed with circles on Figure 3.3 and 3.4. First one is a type-I BBO crystal that is cut at  $\theta = 29^\circ$  and  $\phi = 90^\circ$ . Its dimensions are  $7 \times 7 \times 0.5$  mm. It has  $\lambda/4$  anti-reflection (AR) coatings at the input and the output. The ranges of AR coatings at the input and the output are 700-900 nm and 350-450 nm respectively. This crystal is used for second harmonic generation to pump the nondegenerate OPA, and for parametric amplification in the degenerate one.

The second crystal is a type-II BBO crystal that is cut at  $\theta = 40^\circ$  and  $\phi = 0^\circ$ . Its dimensions are  $7 \times 7 \times 2$  mm. It has AR coatings that are the same as the previous crystal described. This crystal is used for parametric amplification in the nondegenerate OPA.

The second crystal is a type-I BBO crystal that is cut at  $\theta = 51^\circ$  and  $\phi = 90^\circ$ . Its dimensions are  $6 \times 6 \times 0.3$  mm. This crystal is used for second harmonic

generation to pump degenerate OPA. Actually this is our autocorrelator's BBO; on the phase matching curve its angle corresponds to a wavelength of 510 nm for the fundamental. By rotating the crystal about  $20^\circ$  we can achieve frequency doubling at 830 nm using this crystal.

### 3.3 Second Harmonic Generation

Second harmonic generation is an important part of our experiment since it is used to generate our pump beam. Figure 3.5 shows the experimental setup for second harmonic generation. The laser output is focused with the lens (L1) into the type-I BBO crystal. Focusing is necessary to increase the intensity of the fundamental beam at the BBO crystal for efficient conversion to second harmonic. Another lens (L2) is used to collimate the fundamental and the second harmonic. L1 and L2 are fused silica plano-convex lenses that are AR coated for 830nm and 415 nm, respectively. Our laser output is *p*-polarized (parallel to the plane of the optic table) therefore, due to the nature of type-I phase matching the second harmonic is *s*-polarized (perpendicular to the plane of the optic table). A dichroic beam splitter (DBS) is used to separate the fundamental and the second harmonic. We use a type-I BBO crystal at  $\theta = 90^\circ$  and  $\phi = 29^\circ$  whose thickness is 0.5 mm. The effective nonlinear coefficient of the crystal at this angle is 1.61 pm/V. The laser output has a wavelength of 830 nm, resulting in a second harmonic beam generated at 415 nm.

To calculate the expected power of the generated second harmonic we have used the plane wave theory. The conversion efficiency to the second harmonic is defined as

$$\eta \equiv \frac{I_{2\omega}(L)}{I_\omega(0)} = \tanh \xi \quad (3.7)$$

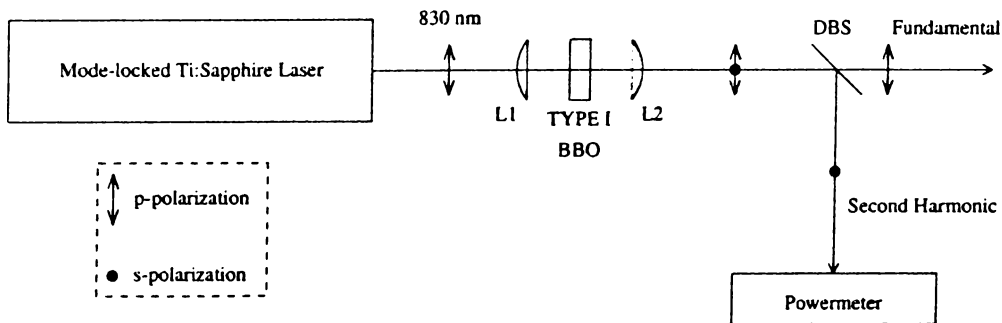


Figure 3.5: Experimental setup for second harmonic generation.

where  $\xi$  is given by the Equations (2.56) and (2.57). To calculate the conversion efficiency correctly  $I_{\omega}(0)$  is taken as the instantaneous peak intensity of the fundamental beam at the input of the crystal. Since the laser output has Gaussian distribution in the transverse plane the intensity profile is not uniform. The most of the power of the laser output is confined into the beam radius and we can think the instantaneous peak intensity as

$$I_{\omega}(0) = \frac{P_{peak}}{\pi W^2} \quad (3.8)$$

where  $P_{peak}$  is the instantaneous peak power of the laser and  $W$  is the beam radius [16] in the crystal. We assume that the intensity distribution is uniform within the beam radius and zero elsewhere ignoring the Gaussian beam profile.

In birefringent crystals  $\mathbf{D}$  and  $\mathbf{E}$  vectors are not parallel to each other if the propagation is not along one of the principal axes. This results in an effect known as walk-off [16] that causes the beams to walk away from each other as they propagate in the crystal. As a result, a limit to the length of the interaction is introduced. The interaction length determined by walk-off depends on the beam radius in the crystal and cannot be ignored if it is less than the crystal length. For the type-I BBO crystal used in this setup, the walk-off angle between the fundamental and the second harmonic is calculated as  $3.8^\circ$ .

To demonstrate the effect of walk-off in second harmonic generation, we experimented with lenses with different focal lengths. First we used lenses with 1 cm focal lengths for L1 and L2. For this case, the beam diameter in the crystal is  $14,5 \mu\text{m}$  (calculated), which results in an effective length of 0.22 mm. Figure 3.6 shows the average power of the second harmonic beam as a function of the average power of the fundamental beam at the input of the crystal when the focal length of both lenses are 1 cm.

When we increase the focal length of L1 the beam radius inside the crystal increases, accounting for an increase in the effective length determined by walk-off in the crystal. Although the effective length increases, the conversion efficiency is less for this configuration, since the conversion is strongly dependent on the intensity of the fundamental beam. To observe this effect, we used lenses with focal lengths of 2.5 and 5 cm for L1. Figure 3.7 and 3.8 shows the conversion to the second harmonic using these lenses. There is a considerable decrease in the conversion to the second harmonic. For both configurations, the effective interaction length is calculated to be more than the crystal length, therefore the interaction length is the length of the crystal.



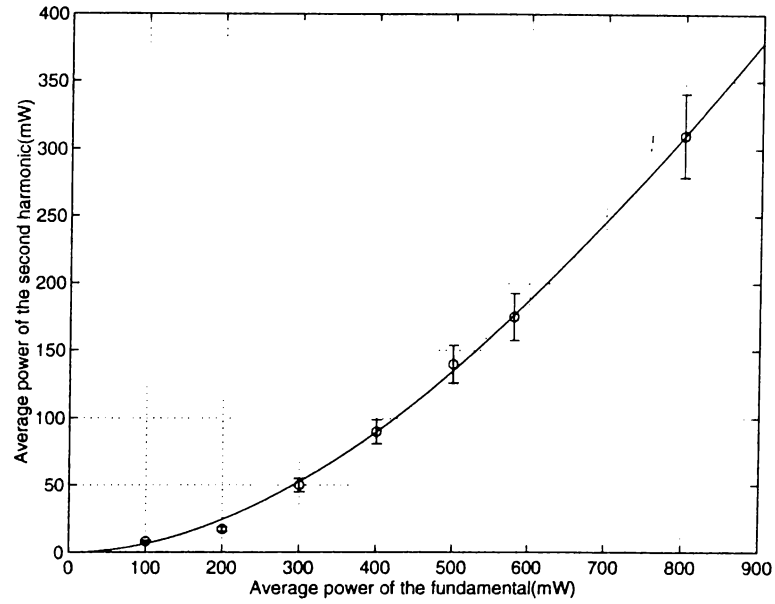


Figure 3.6: Average power of the second harmonic as a function of the average power of the fundamental at the input of the crystal when the focal length of L1 is 1 cm.

For the setup where the focal length of L1 is 1 cm, the average power of the second harmonic is 300 mW for a 800 mW average power of the fundamental at the input of the crystal. This corresponds to a conversion efficiency of 38%. The pulswidth of the fundamental is measured to be 140 fs whereas it is 70 fs for second harmonic.

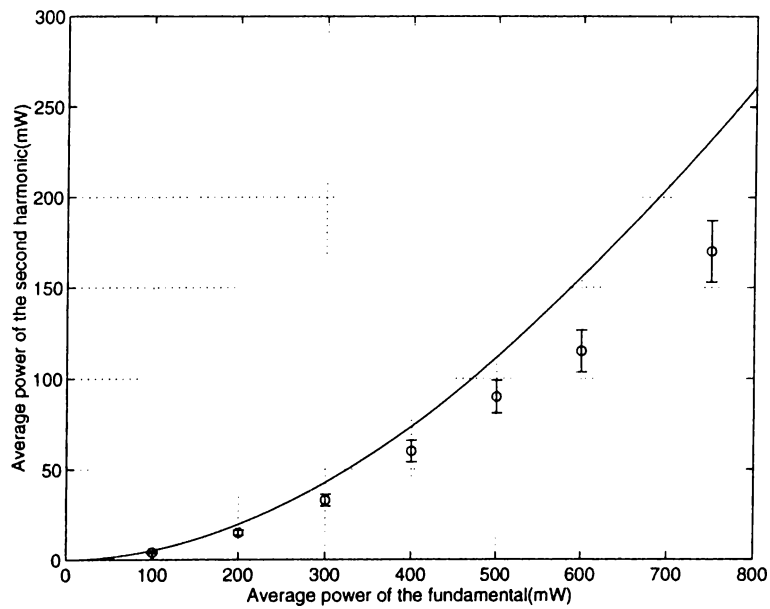


Figure 3.7: Average power of the second harmonic as a function of the average power of the fundamental at the input of the crystal when the focal length of L1 is 2.5 cm.

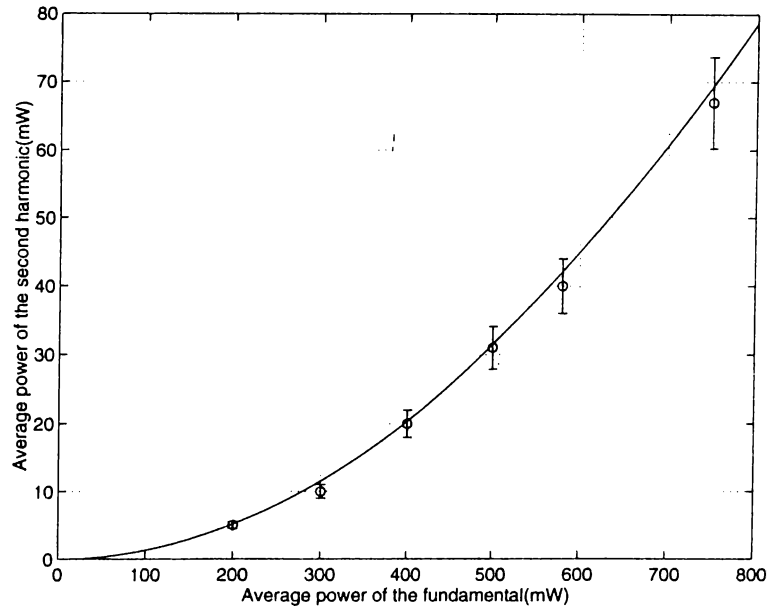


Figure 3.8: Average power of the second harmonic as a function of the average power of the fundamental at the input of the crystal when the focal length of L1 is 5 cm.

## 3.4 Optical Parametric Amplification

Although plane wave analysis together with the concept of effective length due to walk-off provides a sufficiently accurate model for second harmonic generation in our experiments, this is not powerful enough approach for investigating femtosecond optical parametric amplification. There are a number of complications that the model should handle, some of which are due to the ultrafast nature of the experiments, and others are due to the Gaussian transverse profiles of the beams. All of these effects have to be taken into account in a comprehensive model of our OPA experiments.

### 3.4.1 The Pump Beam

The second harmonic at 415 nm is used to pump our optical parametric amplifiers. The frequency doubling part of our experiment is described in detail in Section 3.3. We have chosen the focal lengths of L1 and L2 as 1 cm since the conversion efficiency is maximum with these lenses. Figure 3.9 shows the beam geometry using focused Gaussian beams and a type-I BBO crystal.

Ideally the fundamental and the second harmonic are both Gaussian beams, with the beam waist of the second harmonic being  $1/\sqrt{2}$  of the beam waist

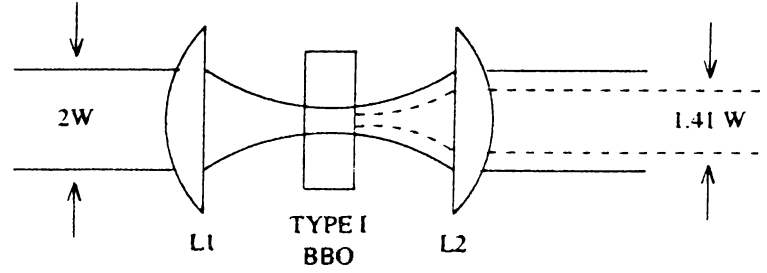


Figure 3.9: Generation of the pump beam using focused Gaussian beams and a type-I BBO crystal. The dashed line shows the beam waist of the second harmonic which is  $1/\sqrt{2}$  of the beam waist of the fundamental. Both the fundamental and the second harmonic have the same confocal distance.

of the fundamental. Both the fundamental and the second harmonic beams have the same confocal distance. However, when lenses with relatively small focal lengths are used the resulting second harmonic does not have a circular transverse profile. This is due to the finite acceptance angle of the crystal [12]. This acceptance angle is narrower in one transverse direction than the other in BBO. As a result the transverse profile of the second harmonic is elliptical.

The lenses L1 and L2 are manufactured from fused silica which is a relatively low dispersion glass. However, fused silica still has some dispersion and hence the focal length of the lenses are wavelength dependent. As a result we cannot achieve perfect collimation for the fundamental and the second harmonic with L2 at the same time. This results in a slight phase front mismatch at the OPA.

### 3.4.2 Parametric Amplification Using Focused Gaussian Beams

The plane wave theory of parametric amplification outlined in Chapter 2 is an idealization since it is impossible to generate plane waves. Most lasers produce Gaussian beam outputs, therefore we have to work with Gaussian beams [15]. Gaussian beams are characterized by their confocal distance  $z_0$ . For a Gaussian beam whose confocal length is  $z_0$  and propagating along the  $z$  direction, the intensity distribution is given by the equation [16]

$$I(x, y, z) = \frac{2P}{\pi W^2(z)} \exp \left[ -\frac{2(x^2 + y^2)}{W^2(z)} \right] \quad (3.9)$$

where  $P$  is the optical power and  $W(z)$  is the beam radius defined as

$$W(z) = W_0 \left[ 1 + \left( \frac{z}{z_0} \right)^2 \right]^{1/2} \quad (3.10)$$

$W_0$  is called the beam waist and is related to the confocal distance by the equation

$$W_0 = \left( \frac{\lambda z_0}{\pi} \right)^{1/2} \quad (3.11)$$

Our optical parametric amplifiers consists of two lenses, and a BBO crystal. The collimated beams of the pump and the signal are focused into the BBO crystal with the first lens and they are recollimated at the output. Both the pump and the signal beams have Gaussian distributions in the BBO crystal. At the center of the pump beam, where the intensity reaches to its maximum value, we have maximum amplification, whereas the nonlinear interaction is less when we deviate from the center.

We can write the transverse intensity profiles of the pump and the signal beams at the input of the crystal as

$$I_p(x, y, 0) = I_{p0} \exp \left[ -\frac{2(x^2 + y^2)}{W_p^2} \right] \quad (3.12)$$

$$I_s(x, y, 0) = I_{s0} \exp \left[ -\frac{2(x^2 + y^2)}{W_s^2} \right] \quad (3.13)$$

where  $W_p$  and  $W_s$  are the beam waists of the pump and the signal, respectively. If we assume that the phase fronts of the pump and the signal perfectly match and the length of the crystal is smaller than the confocal length of the Gaussian beams, (i.e. the beam radius of the pump and the signal stays constant in the length of interaction), the intensity profile of the signal at the output of the degenerate optical parametric amplifier can be written as [17]

$$I_s(x, y, L) = I_s(x, y, 0) \exp(\pm \kappa(x, y)L) \quad (3.14)$$

for  $\pm\pi/2$  phase difference where  $L$  is the length of the crystal and

$$\kappa^2(x, y) = \frac{2\omega^2 d^2 I_p(x, y)}{\epsilon_0 n_s^2 n_p c^3}. \quad (3.15)$$

For the nondegenerate case the intensity profile of the signal at the output is

$$I_s(x, y, L) = I_s(x, y, 0) \cosh^2(\kappa(x, y)L) \quad (3.16)$$

which is independent of phase. To calculate the gain of our amplifier we have to look at the ratio of the input and output powers and calculate the gain of the amplifier using

$$g = \frac{\int I(x, y, L) dx dy}{\int I(x, y, 0) dx dy}. \quad (3.17)$$

### 3.4.3 Effect of Group Velocity Mismatch

The different group velocities experienced by the signal and pump pulses play an important role in the OPA. In the presence of dispersion, the group velocity of pulses propagating at  $\lambda_0$  can be written as [16]

$$v = \frac{c}{N} \quad (3.18)$$

where

$$N = n - \lambda_0 \left. \frac{dn}{d\lambda} \right|_{\lambda=\lambda_0} \quad (3.19)$$

where  $n(\lambda)$  describes the wavelength dependence of the refractive index. The signal and pump pulses, being at different wavelengths, propagate with different velocities in the crystal. This mismatch causes the pump and the signal pulses to drift away from each other while propagating in the crystal. This phenomenon, which is known as the group velocity mismatch, is very important and limits the interaction length of the parametric amplification considerably if femtosecond pulses are used [18].

### 3.4.4 Detection of Ultrashort Pulses

The output signal of the degenerate optical parametric amplifier is detected using a high speed photodetector (Thorlabs 201/579-7227) with a risetime smaller than 1 ns when terminated with a  $50 \Omega$  resistance. This detector is silicon  $p-i-n$  photodiode and its wavelength range is 300–1100 nm.

The 1 ns risetime of this photodiode is not fast enough to detect pulses at the order of 100 fs. Because of this, the pulse shapes that are seen on the oscilloscope are not the actual shapes of the laser output pulses, but the impulse responses of the photodetector. For this reason, the peak of the pulses that are seen on the oscilloscope are proportional to pulse energies, and not the peak pulse power. Therefore, the gain of the OPA that we measure using this detector is

$$g = \frac{\text{output pulse energy}}{\text{input pulse energy}}. \quad (3.20)$$

On the other hand, for pulses with pulsewidths greater than 1 ns, the gain that we measure would be

$$g = \frac{\text{output peak pulse power}}{\text{input peak pulse power}}. \quad (3.21)$$

This is also an important fact that needs to be taken into account. The gain provided by the pump is less at the tails of the pulse whereas it is maximum at the peak. Since it is not possible to use a fast photodiode to resolve femtosecond pulses, we are not able to see the shape of the output pulse and observe that it is less amplified at the tails and more amplified at the peak, but can only measure the time integral of the pulse, i.e. the pulse energy.

### 3.4.5 Degenerate Optical Parametric Amplification

Figure 3.10 shows the experimental setup for degenerate optical parametric amplification. The laser output is focused with a lens (L1) into the 0.3 mm type-I BBO crystal. A similar lens (L2) is used to collimate the fundamental and the second harmonic. A dichroic beam splitter (DBS1) is used to separate the fundamental and the second harmonic. A half-wave plate (HWP) and a polarizing beam splitter (PBS) pair is used to adjust the power level of the signal and keep the *s*-polarization. Using another dichroic beam splitter (DBS2) the pump and signal beams are combined. The laser produces pulses

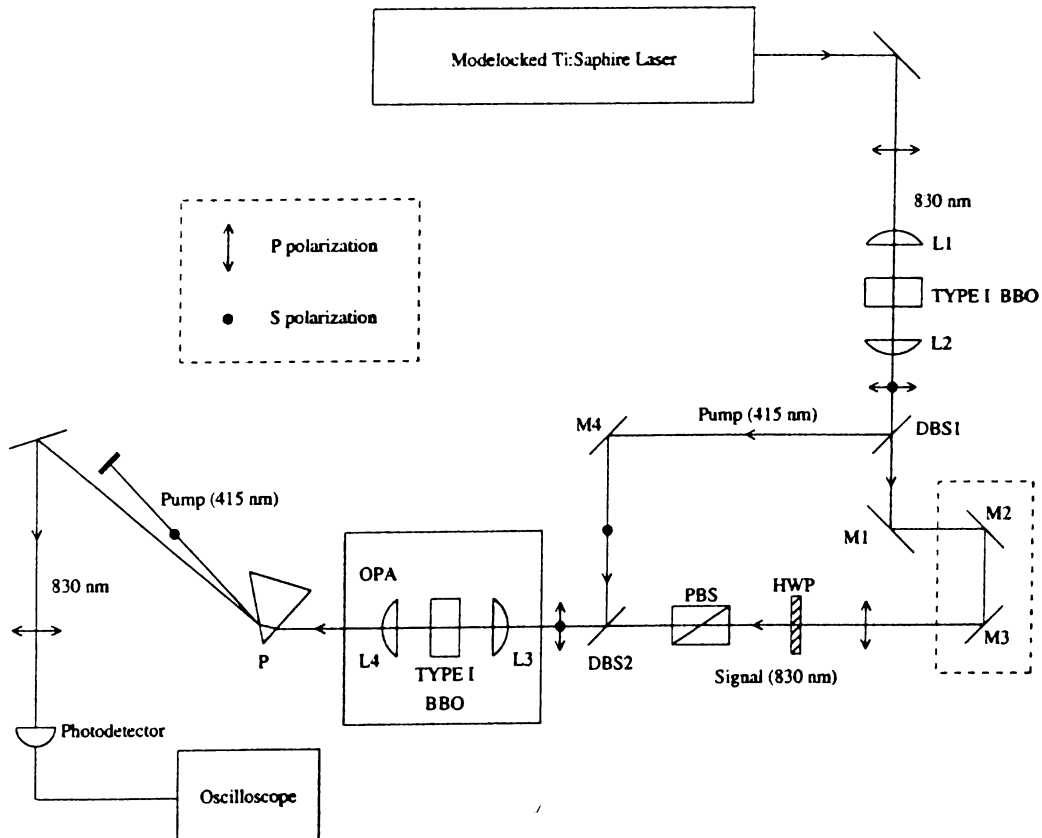


Figure 3.10: Experimental setup for degenerate optical parametric amplification.

on the order of 100 fs which means that their length in space are about  $30 \mu\text{m}$ . In order to have the signal and pump pulses to be synchronous after DBS2, the optical path lengths experienced by the signal and the pump pulses should be equal to each other. To achieve this, two turning mirrors (M2 and M3) are positioned on a translation stage that is carefully adjusted. Two lenses (L3 and L4) and a 0.5 mm type-I BBO crystal forms our degenerate OPA. The pump and the signal are separated from each other at the output by the use of a dispersing prism (P). The signal is detected using a photodetector which is connected to an oscilloscope. L3 and L4 are fused silica plano-convex lenses that are AR coated for 415 nm and 830 nm respectively. Both of their focal length is 2.5 cm.

Effective nonlinear coefficient of the BBO crystal used in optical parametric amplifier is 1.61 pm/V. The walk-off angle between the pump and the signal beams is  $3.8^\circ$ . The group velocity mismatch between the pump and the signal beams is calculated to be

$$\frac{1}{v_{gp}} - \frac{1}{v_{gs}} = 175.7 \text{ fs/mm.} \quad (3.22)$$

Because of dispersion in fused silica, L3 cannot focus the signal and the pump beams onto the same point. The pump and the signal beam waists are separated by 1.2 mm (measured) along the propagation axis due to dispersion in the focusing lens. The beam waists of the signal and the pump are  $18.5$  and  $13.1 \mu\text{m}$ , respectively. At the waist of the pump beam, the signal beam has a radius of  $26.2 \mu\text{m}$ . Figure 3.11 shows the beam geometry within the BBO crystal.

To scan the phase difference between the pump and the signal we introduce small vibrations to one of the components in the setup mechanically and detect the minimum and maximum value of the output signal. The input signal is measured by blocking the pump beam. The ratio of the output to the input

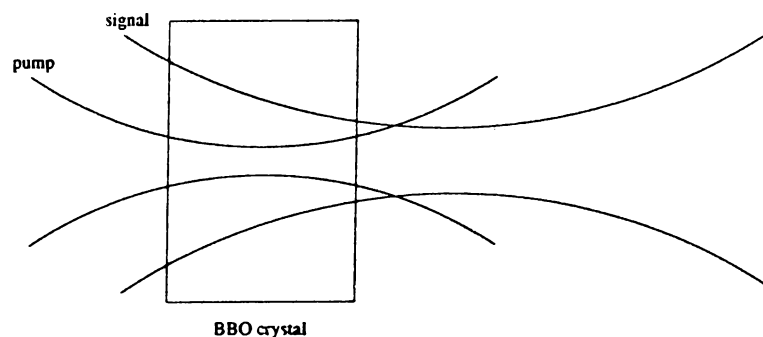


Figure 3.11: Beam geometry within the BBO crystal (not to scale).

signal gives us the amplification and deamplification values of the amplifier.

The theoretical values for amplification and deamplification can be calculated by taking into account the Gaussian nature of the beams, the group velocity mismatch, and time integration over the ultrashort pulses. Deriving analytical solutions for these are quite difficult, therefore it is necessary to develop numerical methods. For our numerical calculations we formed a grid in the  $xy$  plane, and for every grid point, we propagate in time. For doing this, we assumed that the evolution of every point in the grid is due to the plane wave theory. We also assume that the phase fronts of the pump and the signal perfectly match to each other and the walk-off caused by the birefringence of the crystal is negligible. The length of the grid in the  $xy$  plane is  $1\mu\text{m}$  and our time grid is 10 fs. Figure 3.12 shows the theoretical and experimental results of degenerate optical parametric amplifier. The experimental data is in well agreement with the computer simulations. The maximum and minimum measured gains are 1.45 and 0.77 respectively.

The results shown in Figure 3.12 for the nondepleted pump case, where the pump is much stronger compared to the signal and stays constant during the interaction. If the power level of the signal is comparable with the pump, then the photons created (annihilated) at the signal frequency causes a decrease (increase) in the number of the photons at the pump frequency. This situation can also be simulated by a computer program using the property that the sum

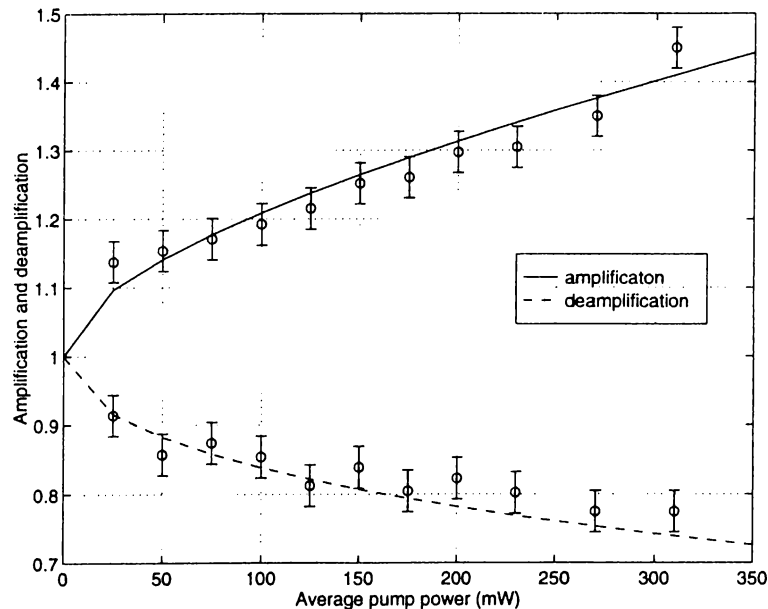


Figure 3.12: Comparison of experimental results with the computer simulation. The solid lines show the amplification and the deamplification according to the computer simulation. The horizontal axis is the average pump power.



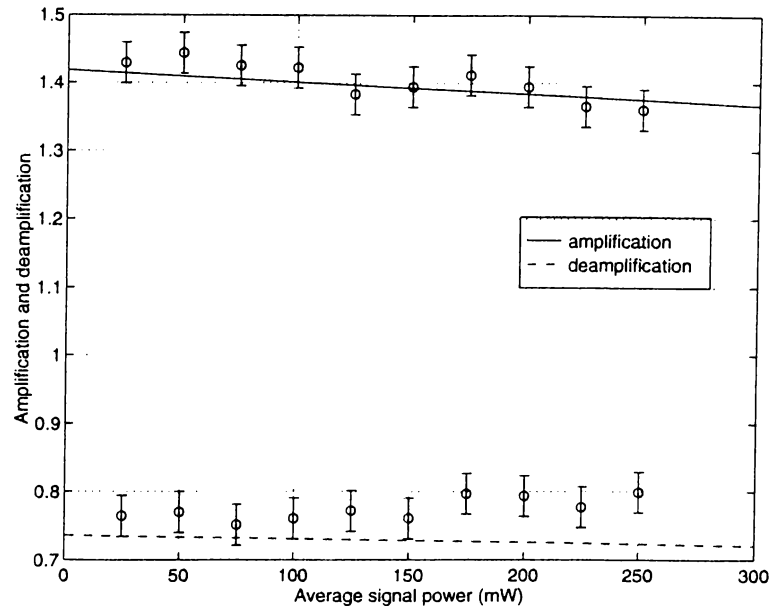


Figure 3.13: Amplification and deamplification response of degenerate optical parametric amplifier for different power levels of the signal.

of the intensities of the signal and the pump fields stay constant during the interaction (Manly-Rowe relations [11]), i.e. a change in the intensity level of the signal beam causes a change in the intensity level of the pump beam in such a way that the total intensity during the interaction stays constant.

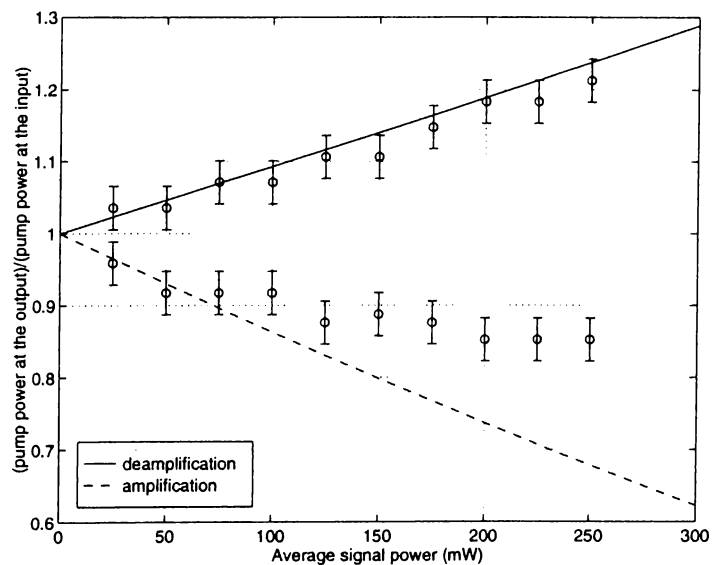


Figure 3.14: Ratio of the pump power at the output to the pump power at the input for degenerate optical parametric amplifier for amplification and deamplification responses.

Figure 3.13 shows the amplification and deamplification responses of degenerate optical parametric amplifier for different values of input signal power. The average pump power is 310 mW. As we increase the signal power, the amplification decreases as it is expected. Figure 3.14 shows the ratio of the pump power at the output to the pump power at the input. For the amplification case there is a decrease in the pump power whereas it increases for the deamplification case. The experimental data does not fit very well to the numerical calculations as the signal power level is increased, but it is acceptable when the approximations that we have made and the precision of the experimental data are taken into account.

### 3.4.6 Nondegenerate Optical Parametric Amplification

For the OPA to be nondegenerate, the signal and the idler should be distinguishable from each other. Nondegeneracy in optical parametric amplification can arise due to three reasons. These are the frequencies, directions of propagation, and polarizations of the signal and the idler beam. To obtain nondegeneracy using different signal and idler frequencies is not practical in our experiments since our pump beam is generated using second harmonic generation. If the signal and idler do not have the same direction of propagation, which states that they have different  $\mathbf{k}$  vectors, this results in a noticeable decrease in the interaction length and complicates phase matching. The most practical way to achieve nondegeneracy in optical parametric amplifiers is to use orthogonally polarized beams for the signal and the idler. This is done by using a type-II crystal in the optical parametric amplifier.

Figure 3.15 shows the experimental setup for nondegenerate optical parametric amplification. In the optical parametric amplifier we use a 2 mm type-II BBO crystal. The effective nonlinear coefficient of the type-II BBO crystal is 1.15 pm/V. At the output of the optical parametric amplifier the signal and the idler have orthogonal polarizations because of the nature of type-II phase matching. A polarizing beam splitter (PBS2) is used to separate the signal and idler beams.

For the nondegenerate optical parametric amplifier there are two factors which limit the interaction length. These are walk-off and group velocity mismatch. For the type-II BBO crystal the walk-off angles between signal, idler,

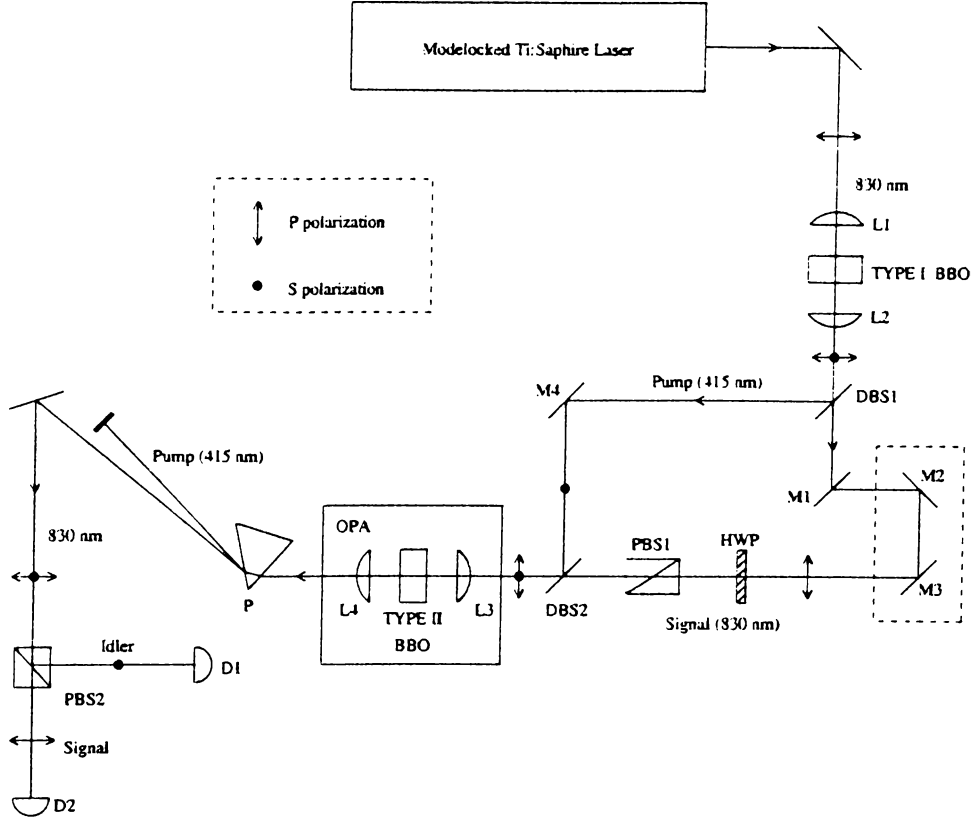


Figure 3.15: Experimental setup for nondegenerate optical parametric amplification.

and pump are calculated to be

$$\alpha_{ps} = 0.22^\circ \quad (3.23)$$

$$\alpha_{pi} = 4.36^\circ \quad (3.24)$$

$$\alpha_{si} = 4.13^\circ \quad (3.25)$$

where the subscripts  $p$ ,  $i$ , and  $s$  stands for pump, idler, and signal waves, respectively. These angles are calculated for a geometry where the signal and the pump have the same polarization, and the polarization of the idler is orthogonal to them. For the same configuration, the group velocity mismatch between the signal, the idler, and the pump beams are calculated to be

$$\frac{1}{v_{gp}} - \frac{1}{v_{gs}} = 252 \text{ fs/mm} \quad (3.26)$$

$$\frac{1}{v_{gp}} - \frac{1}{v_{gi}} = 70 \text{ fs/mm} \quad (3.27)$$

$$\frac{1}{v_{gs}} - \frac{1}{v_{gi}} = -182 \text{ fs/mm}. \quad (3.28)$$

Both walk-off angle and group velocity mismatch can be taken into account by introducing an effective length, which is the distance where the overlap

between the signal and the pump beams is not lost in space or in time. For the configuration where the signal and the pump has the same polarization, the effect of walk-off is less important, and the interaction length is determined by the group velocity mismatch.

The numerical calculations for the parametric gain of the nondegenerate optical parametric amplifier are made using similar methods to those that are used for the degenerate case. First we determine an effective length of interaction determined by walk-off and group velocity mismatch. Once this length is determined, we assume that the interaction takes place in a crystal of this effective length, ignoring the effects of the space walk-off and group velocity mismatch. Even though this is only a crude approximation, it yields acceptable results in calculating parametric gain.

The parametric gain can be calculated taking into account the Gaussian nature of the beams, and the temporal effects. Figure 3.16 shows the results of the computer simulations for the nondegenerate optical parametric amplifier. The effective length for this configuration is calculated to be 0.4 mm. Experimentally, we measured the value of the parametric gain as 1.018 for an average pump power of 310 mW.

Another configuration for the nondegenerate optical parametric amplifier is possible where the signal and the pump beams have orthogonal polarization.

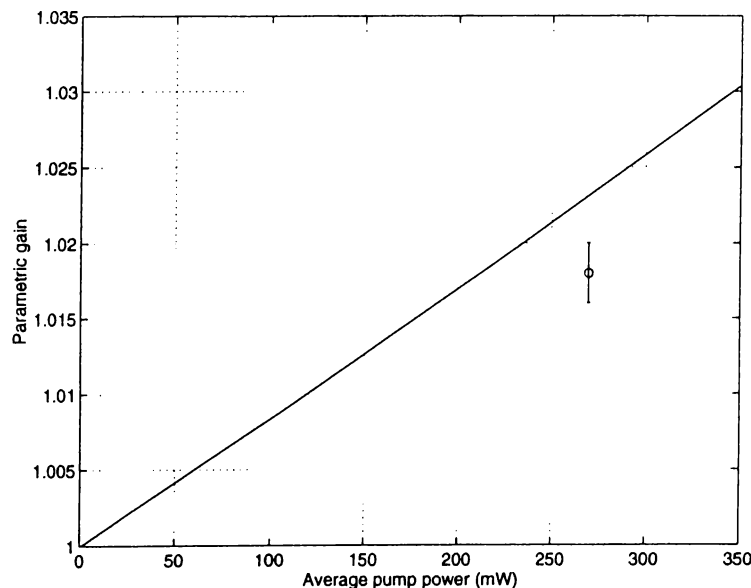


Figure 3.16: Parametric gain of nondegenerate optical parametric amplifier as a function of average power of the pump beam. The signal and the pump beams have the same polarization.

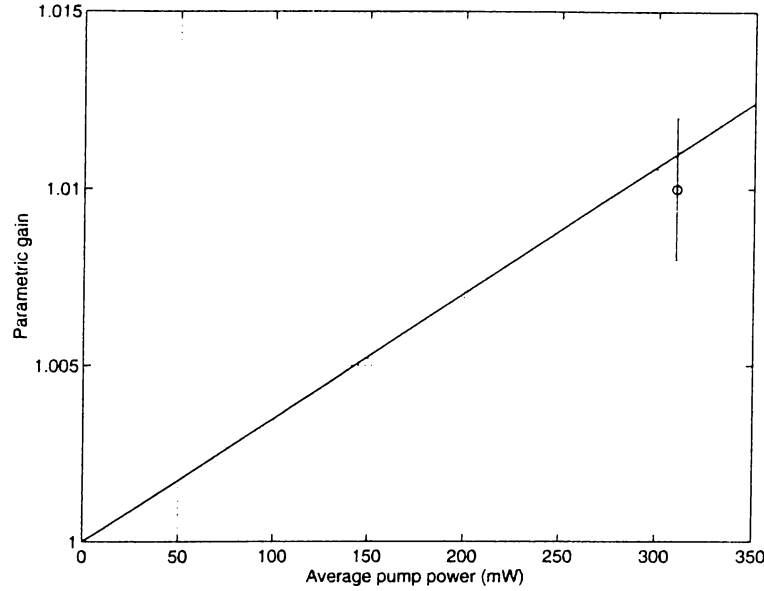


Figure 3.17: Parametric gain of nondegenerate optical parametric amplifier as a function of average power of the pump beam. The signal and the pump beams have orthogonal polarizations.

For this configuration the walk-off angles and group velocity mismatches are the same as the previous case if the subscripts  $s$  and  $i$  are interchanged. The same analysis is carried out to determine the parametric gain of the amplifier. For this configuration the effect of group velocity mismatch is less important and the interaction length is determined by walk-off.

Figure 3.17 shows the results of the computer simulations for the nondegenerate optical parametric amplifier for the case where the signal and the pump have orthogonal polarizations. The effective length for this configuration is 0.27 mm. Experimentally we have measured the value of the parametric gain as 1.01 for an average pump power of 270 mW.

The experimental results show us that nondegenerate optical parametric amplification using a type-II BBO crystal cannot achieve high gain because of the effects of walk-off and group velocity mismatch. We are able to observe parametric amplification but the parametric gain is very small. Recently it has been demonstrated that both phase and group velocity matching can be achieved using noncollinear beams and tilted pulses [18]. Also it has been shown that matching the group velocities by spatial walk-off in collinear three wave interaction is possible using tilted pulses [19].

# Chapter 4

## CONCLUSIONS

This thesis describes our experimental efforts to construct and evaluate femtosecond OPAs based on beta-barium borate crystals. A femtosecond Titanium:Sapphire laser operating at a wavelength of 830 nm was used as the source in these experiments. This laser was frequency doubled with a type-I BBO crystal into the blue. This frequency doubled beam provided the pump to our OPAs, and the remaining fundamental provided the signal input.

We observed that the interaction length in the type-II BBO crystal was limited by walk-off and group velocity mismatch. The ultrafast nature of the pulses from our laser makes GVM particularly important. As a result of this, the gain of our nondegenerate optical parametric amplifier was very low ( $g=1.02$ ). For type-I BBO crystal the effects of walk-off and group velocity mismatch were less, but we still suffered from them. The gain of our degenerate optical parametric amplifier in which we used a type I BBO crystal was better ( $g=1.45$ ) than that of the nondegenerate optical parametric amplifier. This was expected, since the phase sensitive gain of optical parametric amplifiers are greater than phase insensitive gain.

In second harmonic generation, we have achieved 38% conversion efficiency to the second harmonic using a type-I BBO crystal. The resulting output beam profile was elliptical due to different acceptance angles of the BBO crystal at orthogonal transverse directions.

The longer term aim of our experiments is to investigate quantum optical properties of degenerate and nondegenerate optical parametric amplification in the femtosecond regime. This proved to be difficult since the parametric gains

we achieved were not high. We are currently investigating various schemes to increase our parametric gain.

As future work, we are planning to increase the gain of our optical parametric amplifier by correcting the ellipticity of our pump beam and using lenses with smaller focal lengths. Using this setup we hope to be able to generate and measure squeezed states in femtosecond regime. We are also designing a setup to overlap the focus of the pump and the signal beams by using extra wavefront shaping elements. Doing this, we hope to be able to solve the problem of matching the phase fronts of the signal and the pump beams. Another design is a nondegenerate optical parametric amplifier using noncollinear beams for the signal and the pump. Using this setup, we hope to be able to generate twin beams.

## REFERENCES

- [1] T. H. Maiman, *Nature*, vol. 187, p. 493, 1960.
- [2] P. A. Franken, A. E. Hill, C. W. Peters, and G. Weinreich, "Generation of optical harmonics," *Physical Review Letters*, vol. 7, pp. 118-119, 1961.
- [3] C. C. Wang and G. W. Racette, "Measurement of parametric gain accompanying optical difference frequency generation," *Applied Physical Letters*, vol. 6, pp. 169-171, 1965.
- [4] J. A. Giordimane and R. C. Miller, "Tunable coherent parametric oscillation in  $\text{LiNbO}_3$  at optical frequencies," *Physical Review Letters*, vol. 14, pp. 973-976, 1965.
- [5] H. M. van Driel, "Synchronously pumped optical parametric oscillators," *Applied Physics B*, vol. 60, pp. 411-420, 1995.
- [6] Roy J. Glauber, "Coherent and incoherent states of the radiation field," *Physical Review Letters*, vol. 131, pp. 2766-2788, 1963.
- [7] Horace P. Yuen, "Two-photon coherent states of the radiation field," *Physical Review Letters*, vol. 13, pp. 2226-2243, 1976.
- [8] Ling-An Wu, H. J. Kimble, J. L. Hall, and Huifa Wu, "Generation of squeezed states by parametric down conversion," *Physical Review Letters*, vol. 57, pp. 2520-2523, 1986.
- [9] O. Aytür, "Squeezed light and twin beams generation with a Q-switched laser," Ph. D. Thesis, Northwestern University, 1991.
- [10] Orhan Aytür and Prem Kumar, "Pulsed twin beams of light," *Physical Review Letters*, vol. 65, pp. 1551-1554, 1990.
- [11] R.W. Boyd. *Nonlinear Optics*. Academic Press, Inc., San Diego, 1992.



- [12] Richard A. Baumgartner and Robert L. Byer, "Optical parametric amplification," *IEEE Journal of Quantum Electronics*, vol. QE-15, pp. 431-445, 1979.
- [13] P. Kumar "Quantum Properties of Optical Parametric Amplifiers," Short Course 120. Conference on Lasers and Electrooptics, 1995.
- [14] V.G. Dimitriev, G. G. Gurzadyan, and D. N. Nikogosyan. *Handbook of Nonlinear Optical Crystals*. Springer-Verlag, Berlin, 1991.
- [15] G. D. Boyd and D. A. Kleinman, "Parametric interaction of focused gaussian beams," *Journal of Applied Physics*, vol. 39, pp. 3597-3639, 1968.
- [16] Bahaa E. A. Saleh, Malvin Carl Teich. *Fundamentals of Photonics*. John Wiley and Sons Inc., New York, 1991.
- [17] Chonghoon Kim, Ruo-Ding Li, and Prem Kumar, "Deamplification response of a traveling-wave phase-sensitive optical parametric amplifier," *Optics Letters*, vol.19, pp. 132-134, 1994.
- [18] T. R. Zhang, Heung Ro Choo, and Michael C. Downer, "Phase and group velocity matching for second harmonic generation of femtosecond pulses," *Journal of Optical Society of America, Applied Optics*, vol. 29, pp. 3927-3933, 1990.
- [19] R. Danielius, A. Piskarskas, P. Di Trapani, A. Andreoni, C. Solcia, and P. Foggi. "Matching of group velocities by spatial walk-off in collinear three-wave interaction with tilted pulses," *Optics Letters*, vol. 21, pp. 973-975, 1996.